Chapter 4. Structural Setup of the Study Area

4.1 Introduction

On the basis of the geological map of the study area given in chapter 3 (Fig. 3.1), it is apparent that the Champaner terrain shows the presence of versatile rock types yet in a cyclic manner. Though being a smaller extent it represents structural intricacy depicted by means of shapes and trends of various competent rocks intercalated with incompetent litho-units (Fig. 4.1). The present work helped the author to decode the structural complexities present within the Champaner terrain. By using the information from the Survey of India (SOI) topographic sheet and Landsat data (low altitude satellite), the areas showing complex to simple folding pattern have been selected for detail structural mapping. With the help of detailed field work, data of various planar and linear structural elements have been recorded viz. beddings, foliations and lineations. In case of monomineralic rock showing weak foliation signatures, Anisotropy of Magnetic Susceptibility (AMS) analyses has been resorted to decrypt the deformational fabric present within these rocks. The structural attributes obtained from the field work have been plotted on Schmidt Equal Area Stereographic Net to decipher the sequence of folds events and their inter-relationship with one another. In case of regional fold structures, the calculated fold axis through stereographic net is aided by the plots prepared on the basis of lineation data obtained from the field. Based on the inter-relationship of different fold events various interference fold patterns on regional scale have been identified. Along with the derivatives of the fold events, evidences of brittle and ductile shears present within the terrain have been deciphered.

* The part of this chapter is based on our paper published:
(a) Joshi, A U (In-Press) Fold interference patterns in Meso-Proterozoic Champaner Fold Belt (CFB) Gujarat, western India. Journal of Earth System Sciences.
(b) Joshi, A U and Limaye, M A (2018) Rootless calc-silicate folds in granite: An implication towards syn-to-post plutonic emplacement. Journal of Earth System Sciences. 127:67; doi: https://doi.org/10.1007/s12040-018-0968-6.
(c) Joshi, A U and Limaye, M A (2014) Evidences of Syndeformational granitoid emplacement within Champaner group, Gujarat. Journal of M.S.U.S.T, vol.49 No. 1, pp.45-54.

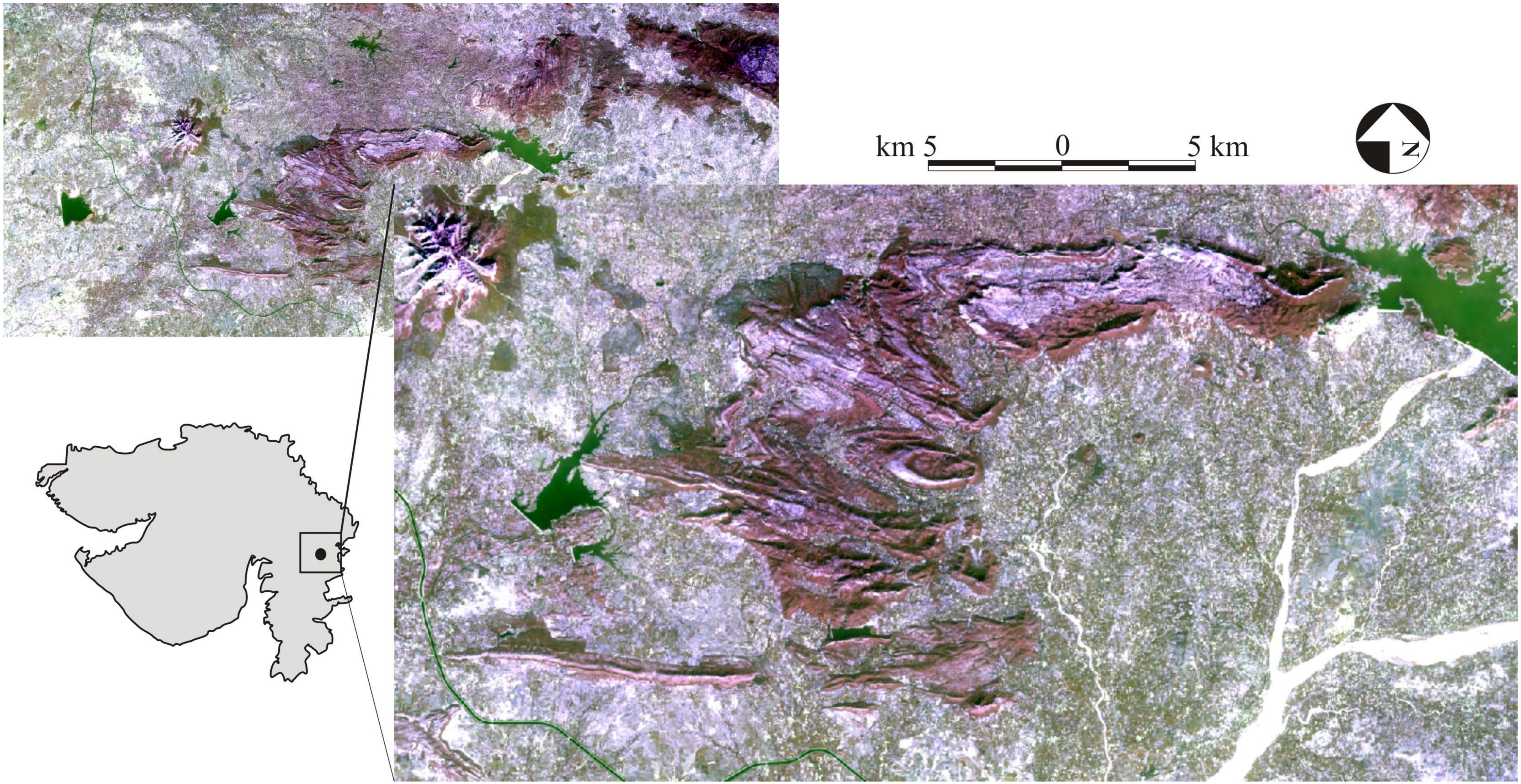

Figure 4.1: Landsat data of the Champaner terrain (Source: USGS-Earth Explorer).

Finally, the complete package of the above evidences has been used to decipher the structural evolution of the Champaner Group and its relationship with the neighbouring Pre-Cambrian stratigraphic units.

On the basis of the structural elements and availability of the outcrop patterns, the Champaner Group has been divided into five sectors (Fig. 4.2). These sectors include: Sector 1: Rustampura to Malabar; Sector 2: Malabar to Pani; Sector 3: Narukot to Wadek; Sector 4: Bhamaria to Kanpur; Sector 5: Isolated patch at Goldungri near Jothwad. The description incorporated in the following pages deals with the geometry of the folds present within each sector and its structural analyses.

4.2 Sector 1: Rustampura to Malabar

The area within this sector shows evidences of three fold events F_1, F_2, F_3 (Fig. 4.3). The northern part of the present sector is characterised by F_1 and F_2 folds, whereas the F_3 folds show their dominance in the eastern and southern part, respectively. The F_1 folds are second order tight on meso-scale, while F_2 folds are first order open comprising on regional scale. The F_1 and F_2 folds demarcate steep to gentle plunge of their folds axes, respectively, with vertical or nearly vertical axial traces. F_3 folds are mainly restricted to vicinity of the granites and show broad open warps developed on kilometre long limbs of F_1 and F_2 folds. The steepness of F_3 fold axis increases in the eastern and southern part of this sector, whereas in the northern and western direction, these exhibit meso-scale kinks.

Based on the data homogeneity, strike persistency and presence of regional scale fold closures, the sector has been divided into six domains (i.e. from domain I to VI).

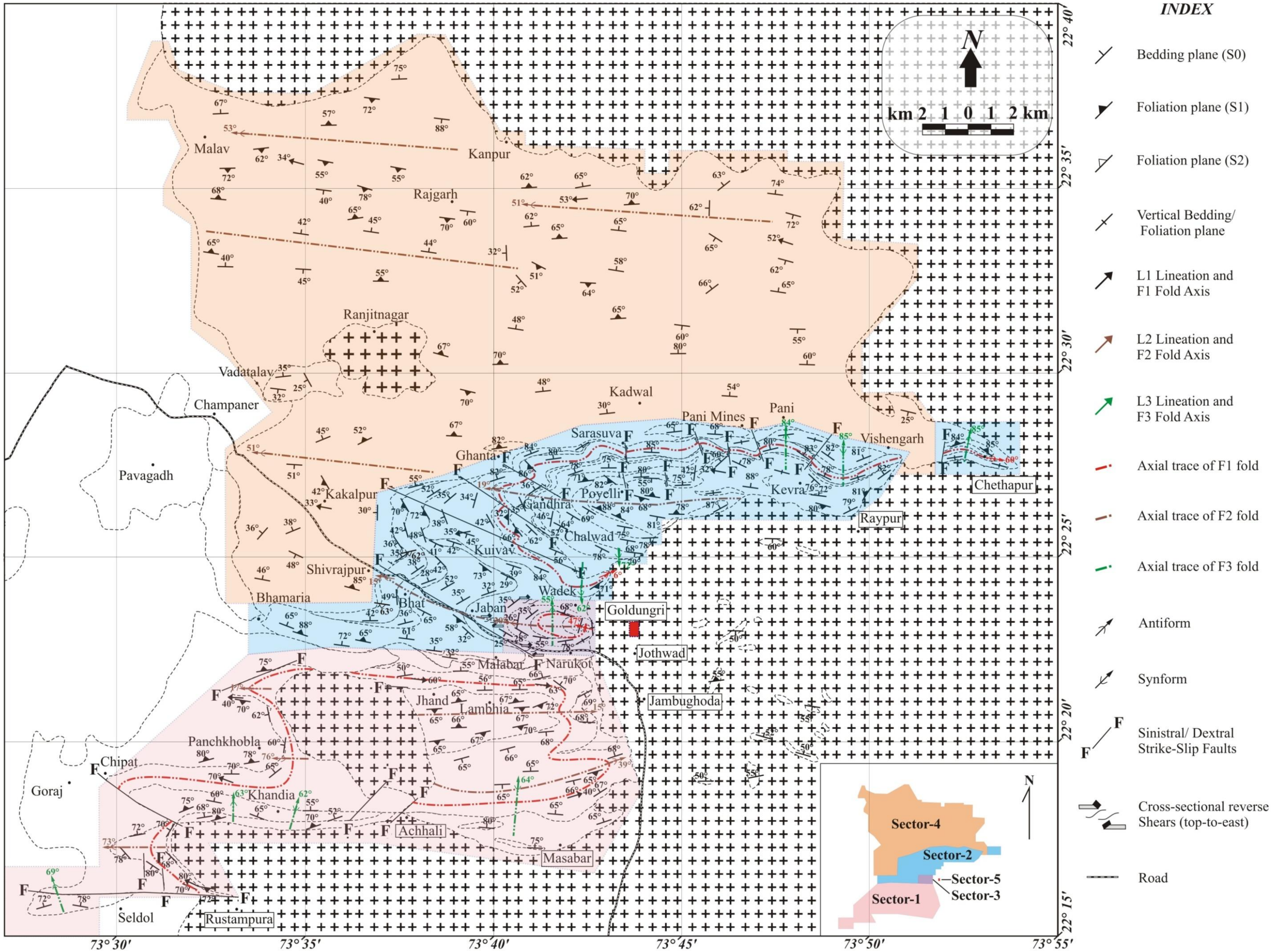

Figure 4.2: Structural Map of the Study area. Modified after Jambusaria, 1970; Gupta et. al., 1997.

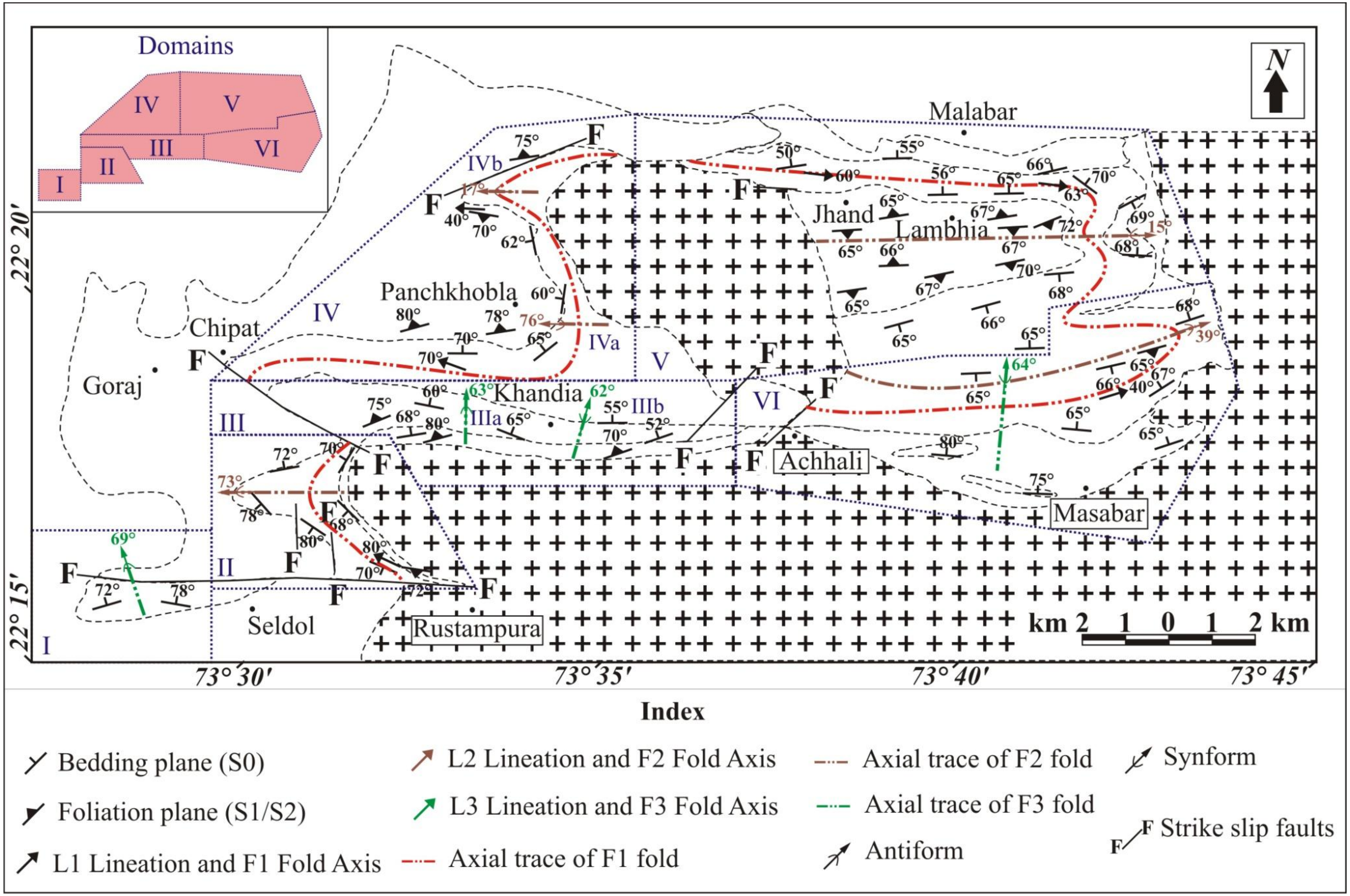

Figure 4.3: Structural Map of Sector 1.

4.2.1 Structural Analyses of Sector 1

Domain I

Domain I is located west of Seldol and represent F_3 antiformal structure on a regional scale, and comprises of quartzites. Structural elements recorded were area bedding plane S_0. Being the rock itself of non-foliated nature, secondary foliation was negligible. The domain represents scarcity of the data because majority of the outcrops were mined extensively for road construction. The contoured π- diagram plotted with the aid of S_0 data suggests that the orientation of the F_3 fold axis in this domain has an attitude of 69^o/ N341^o (Fig. 4.4).

Domain II

Domain II depicts combinations of F_1 and F_2 folds on regional scale and located north of Rustampura village. The bedding plane S_0 observed in this domain was useful in analysing F_1 fold axis, whereas secondary foliation S_1/ S_2 was used to calculate the F_2 axis. There exists slight oblique relationship between the bedding and the foliation, however both show more or less similar amount of dip. The bedding/ foliation in the northern part of the domain II strikes NNE-SSW to NW-SE with northerly dip and swing to attend nearly southerly dip with a strike of N90^o (Fig. 4.4). The calculated fold axis through contoured π- diagram for F_1 folds suggest that the fold axis plunges with an amount of 77^o in the direction of N295^o, whereas the F_2 folds show a plunge of 50^o in the direction of N269^o. The field lineation data of meso-scale F_1 fold axes also matches with the statistically derived F_1 fold axis through stereographic projection. The manifestation of F_2 over F_1 in this domain is the form of steeping of earlier F_1 fold due to refolding to form F_2.

Domain III

This domain lies from east to west of the Khandia village and depicts antiform and synform. The antiformal structure has been designated as sub-domain IIIa, while the synformal structure as sub-domain IIIb. The nature of folds in this domain indicates broad open warps representing F_3 folds. These folds are found to be developed on kilometre long limbs of F_1 and F_2 folds. The bedding shows oblique relationship with the foliation plane. Moreover, the foliation plane is steeper as compared to the bedding. One limb, of the antiformal structure strikes ENE-WSW having dip

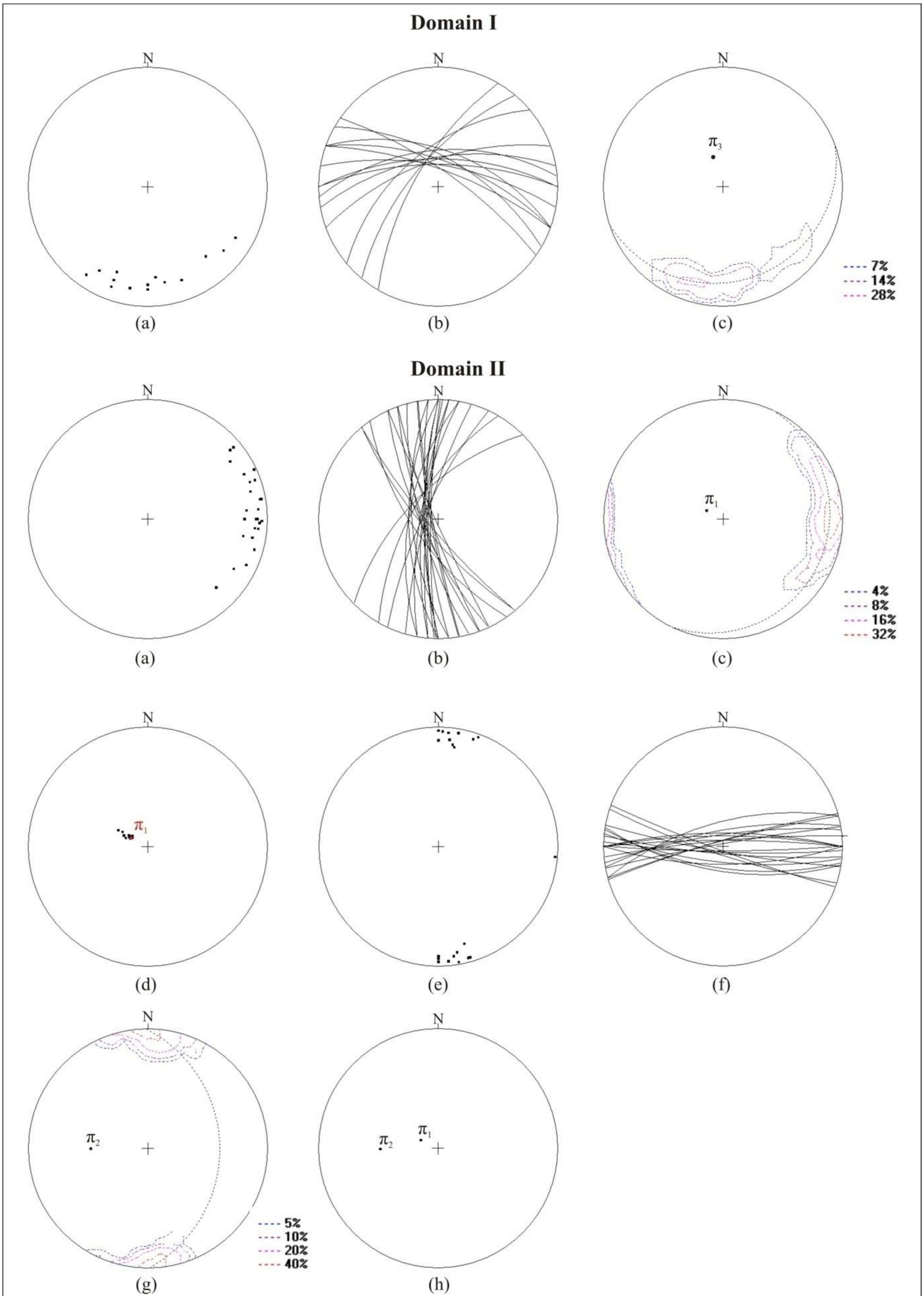

Figure 4.4: **Domain I**: (a) Poles to planes (S0, n=15); (b) Cyclographic plot (S0, n=15); (c) Contoured pie diagram (7, 14, 28% contours per 1% area). **Domain II**: (a) Poles to planes (S0, n=26); (b) Cyclographic plot (S0, n=26); (c) Contoured pie diagram (4, 8, 16, 32% contours per 1% area); (d) Lineation data of F1 (n=10); (e) Poles to planes (S1, S2, n=20); (f) Cyclographic plot (S1, S2, n=20); (g) Contoured pie diagram (5, 10, 20, 40% contours per 1% area); (h) Relationship of F2 over F1.

direction due NNW, whereas the other limb strikes WNW-ESE with dip direction due NNE. The fold axis calculated by plotting S_0 and S_1 planes suggest that the fold plunges due north with an amount of 63^o (Fig. 4.5). The synformal structure has a limb attitude in terms of dip direction ranging from N to NNE with plunge 62^o in the direction of N16^o.

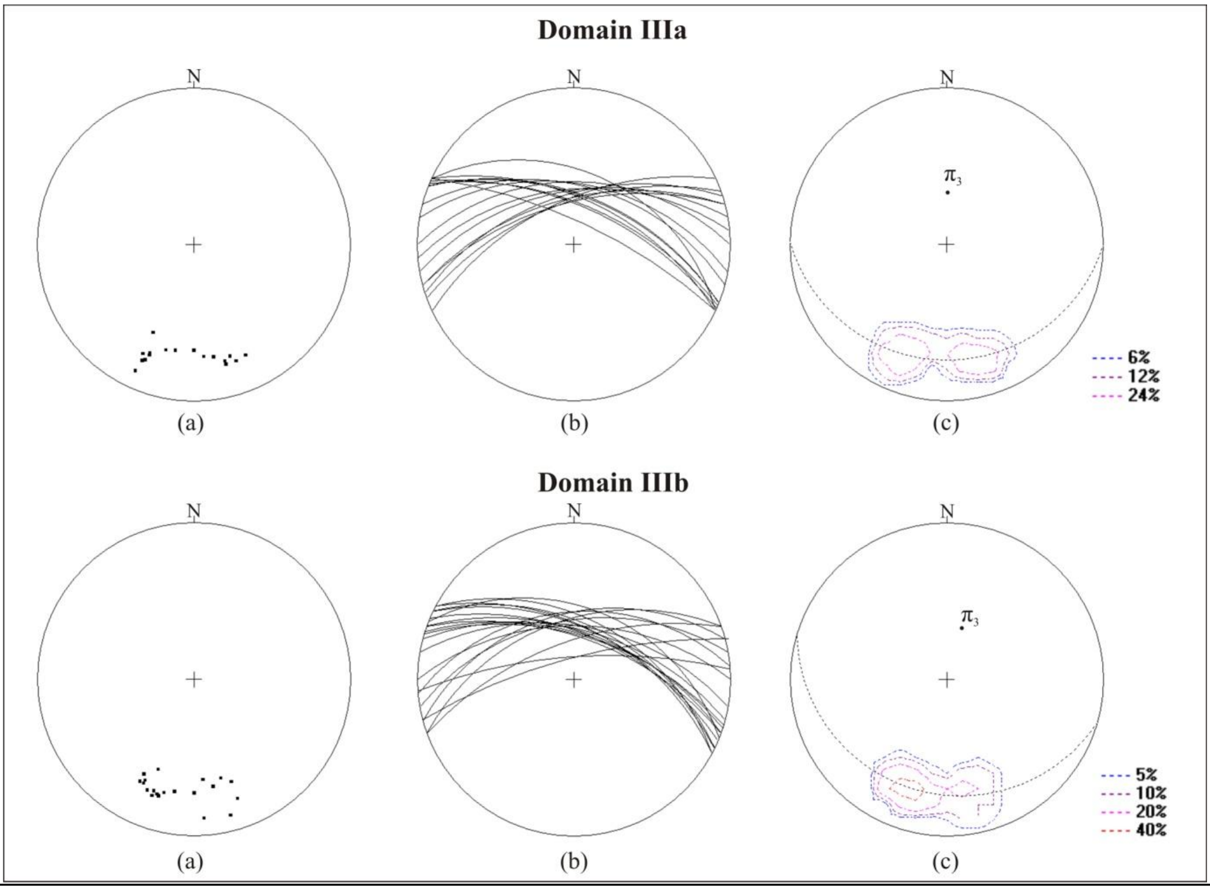

Figure 4.5: **Domain IIIa**: (a) Poles to planes (S0, S1, n=17); (b) Cyclographic plot (S0, S1, n=17); (c) Contoured pie diagram (6, 12, 24% contours per 1% area). **Domain IIIb**: (a) Poles to planes (S0, S1, n=20); (b) Cyclographic plot (S0, S1, n=20); (c) Contoured pie diagram (5, 10, 20, 40% contours per 1% area).

Domain IV

Domain IV has been divided into two sub-domains, i.e. sub-domain IVa and sub-domain IVb. Both lie to the south and the north of the Panchkhobla village, respectively. The Sub-domain IVa consists of steeply plunging synformal structure and display combinations of F_1 and F_2 folds. The structural data recorded from this sub-domain are S_0 and S_1 having sub-parallel relationship with each other. As seen in the previous domain, the secondary foliation S_1 is steeper as compared to the bedding plane S_0. The contoured π- diagram generated using the bedding plane readings for F_1 folds in IVa, suggest that the fold axis plunges due WNW with an amount of 69°. In case of F_2 folds over F_1, depicts vertical axial trace with a plunging fold axis of 76° due western direction (Fig. 4.6). It's quite surprising in this particular sub-domain that the manifestation of F_2 over F_1 has not been responsible in steepening of the earlier fold axis. The probable explanation could be given in this case is that being the sub-domain IVa consist paucity of structural data due to limited exposures, the clear relationship of F_2 over F_1 was unable to derive statistically.

In case of sub-domain IVb, there exists an antiformal structure showing F_2 fold comprising its two limbs and the core. The northern limb of the F_2 fold strikes ENE-WSW direction while the southern limb strikes E-W direction. The contoured π- diagram shows F_2 axis in westerly direction with an amount of 17°. Here, meso-scopic F_1 fold axes obtained through field give plunge of the L_1 lineations as 40° in due N273° (Fig. 4.7). Overall the plunge amount of F_1 gradually increases due to its refolding and has a strong association with the uplift on account of the adjacent granitic intrusion. This fact is better understood when the data of the domain V lying east of the present domain is taken into consideration.

Domain V

The area around Jhand is enveloped by regional scale F_2 folds comprising of quartzites along with meso-scale F_1 folds (Fig. 3.2a). The overall pattern shows series of antiforms and synforms having intermixed granite-gneisses at the core. The bedding plane S_0 within these quartzites strikes E-W to ENE-WSW with variable dip direction having a moderate amount of 50°-65°. The foliation plane within intermixed granite-gneisses exhibit similar trend to that of quartzites and is found to be co-folded with the Champaner meta-sediments. However, meso-scale F_1 folds are found to be missing within the intermixed variety. The structural data recorded from this domain is S_0, S_1, S_2, out of which S_1 and S_2 are virtually parallel to one another. The fold axis of F_1 fold plunges with an amount of 55° in the direction of N97°, where as the F_2 fold axis show a plunge of 15° in the direction of N89° (Fig. 4.8). As discussed in the domain IVb the fold axis of F_2 folds plunges 17° due west, whereas in domain V, the fold axis plunges 15° due east. This fact suggests an imprint associated with F_3 in the central region resulted on account of the granitic intrusion. Moreover, there also exists evidences of meso-scale F_3 warps suggesting N-S deformation within these rocks (Fig. 3.2c).

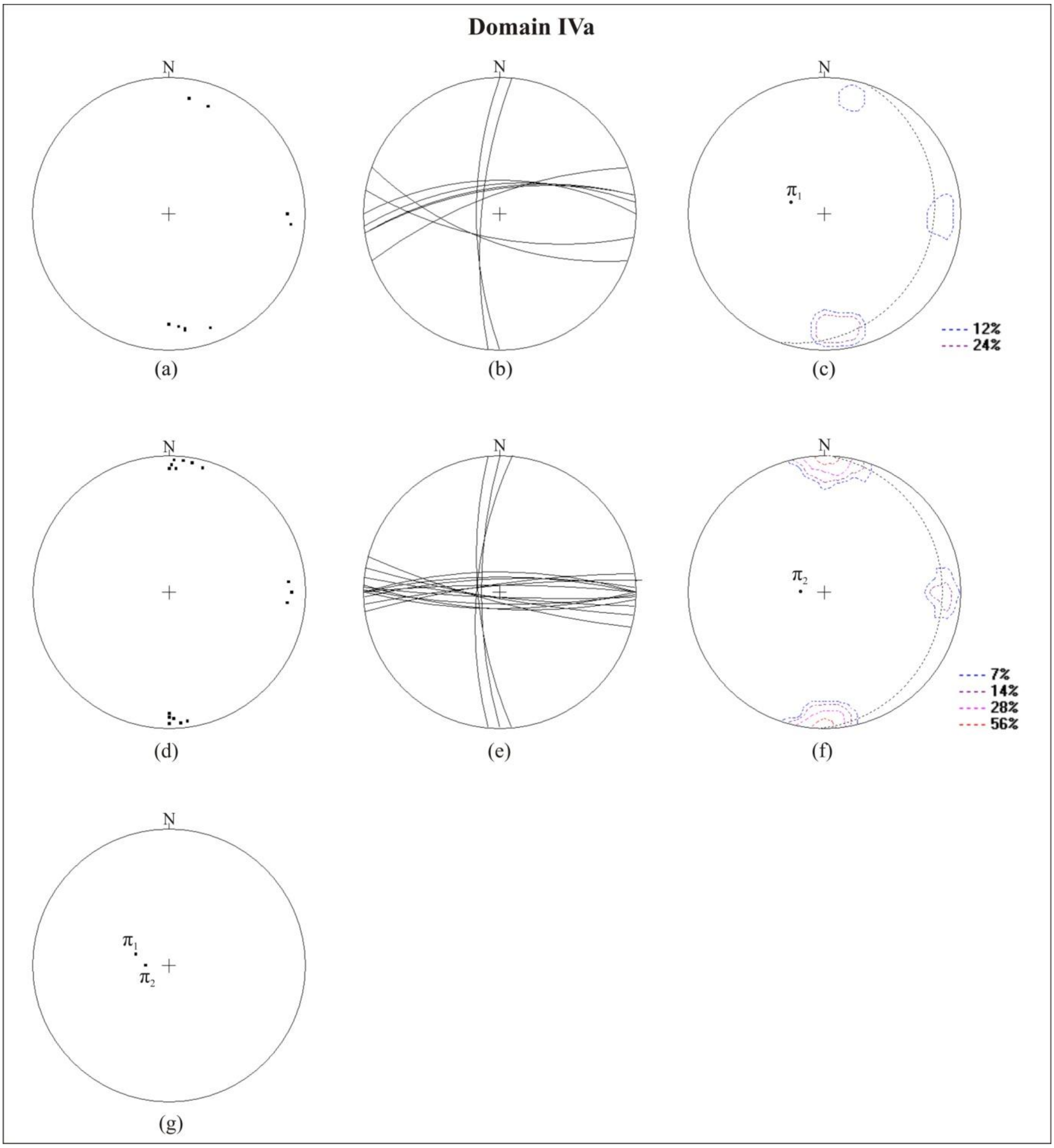

Figure 4.6: **Domain IVa**: (a) Poles to planes (S0, n=09); (b) Cyclographic plot (S0, n=09); (c) Contoured pie diagram (12, 14% contours per 1% area); (d) Poles to planes (S1, n=16); (e) Cyclographic plot (S1, n=16); (f) Contoured pie diagram (7, 14, 28, 56% contours per 1% area); (g) Relationship of F2 over F1.

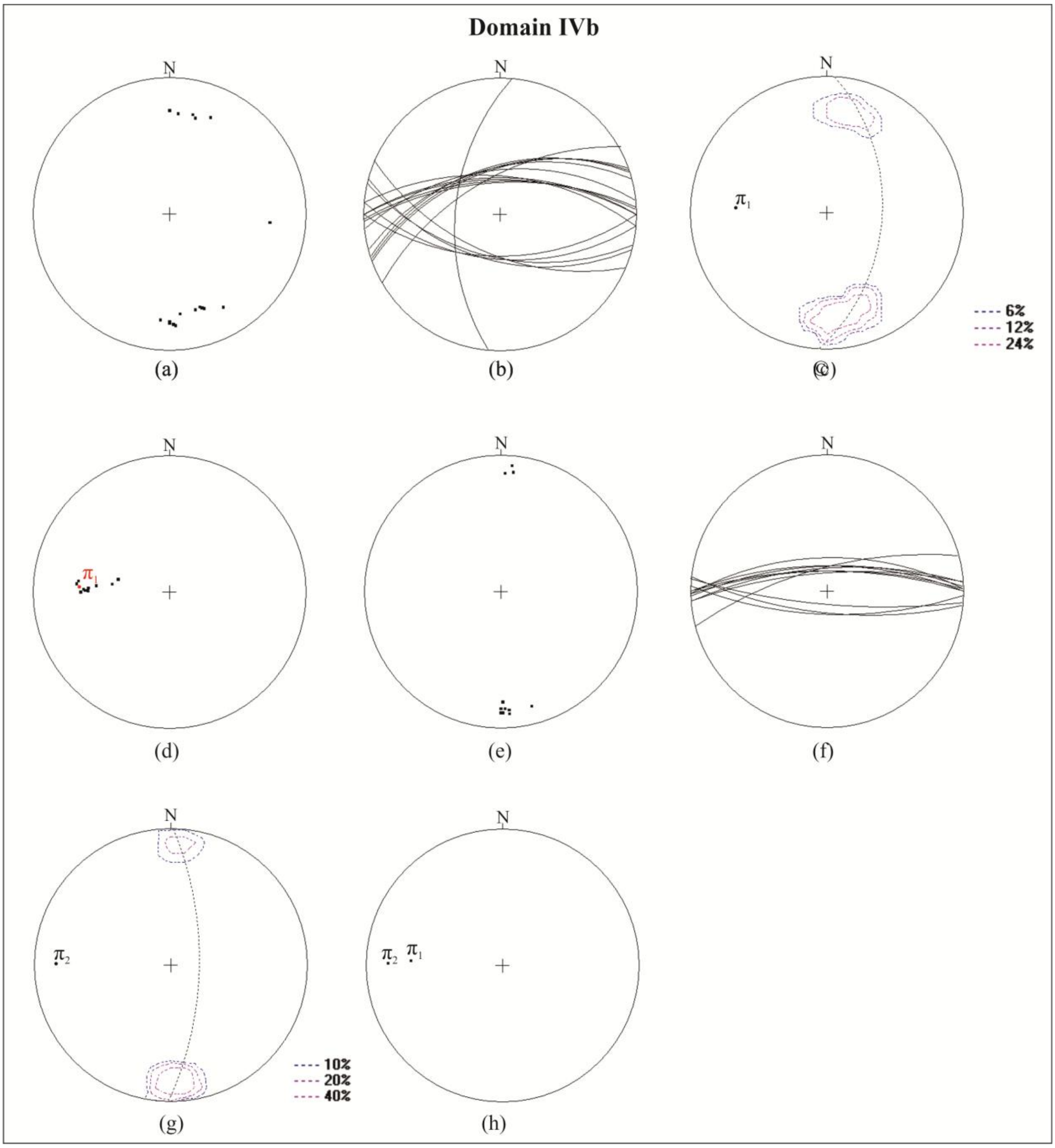

Figure 4.7: **Domain IVb**: (a) Poles to planes (S0, n=17); (b) Cyclographic plot (S0, n=17); (c) Contoured pie diagram (6, 12, 24% contours per 1% area); (d) Lineation data of F1 (n=10); (e) Poles to planes (S1, n=11); (f) Cyclographic plot (S1, n=11); (g) Contoured pie diagram (10, 20, 40% contours per 1% area); (h) Relationship of F2 over F1.

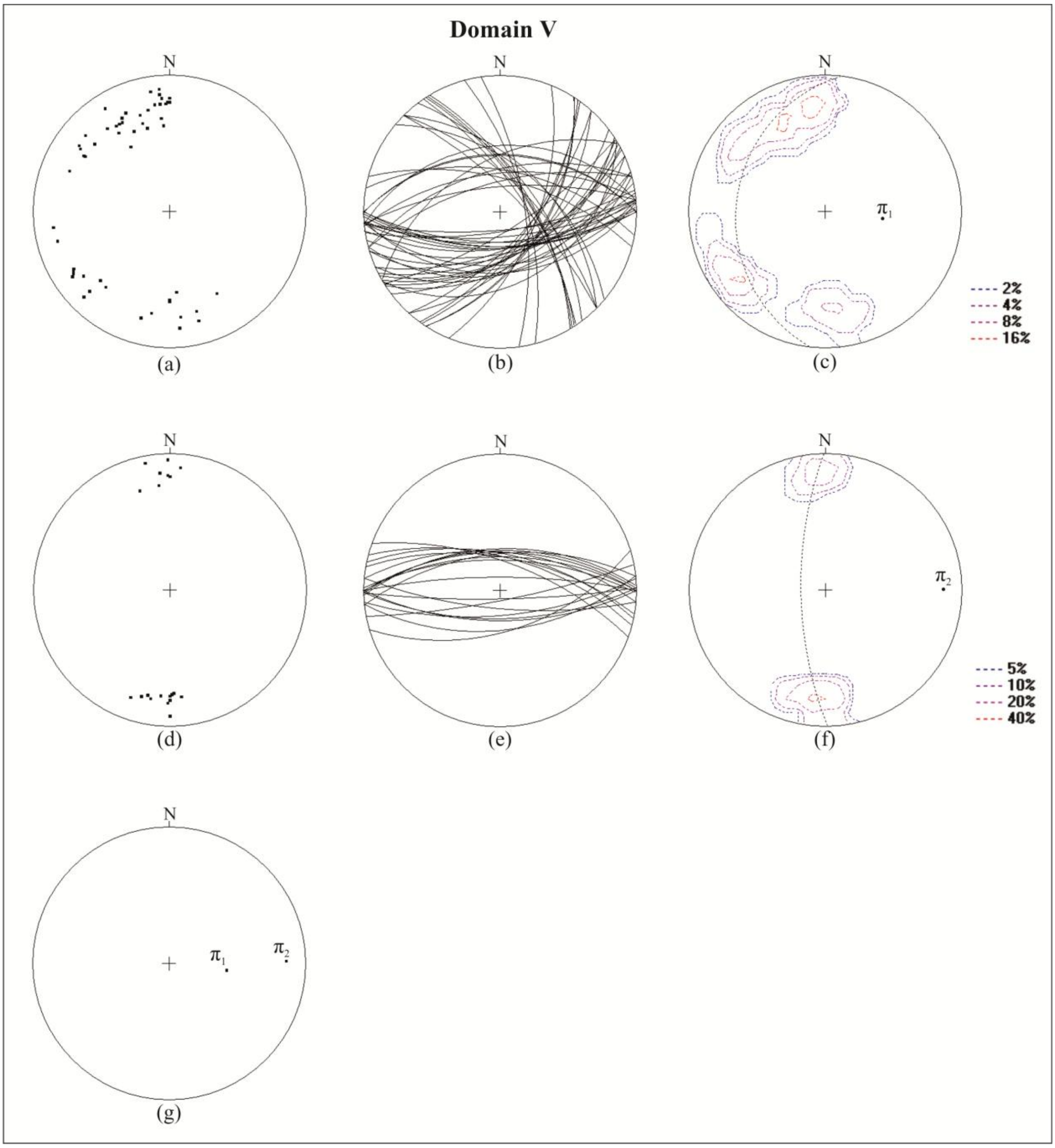

Figure 4.8: **Domain V**: (a) Poles to planes (S0, n=56); (b) Cyclographic plot (S0, n=56); (c) Contoured pie diagram (2, 4, 8, 16% contours per 1% area); (d) Poles to planes (S1, S2, n=20); (f) Cyclographic plot (S1, S2, n=20); (g) Contoured pie diagram (5, 10, 20, 40% contours per 1% area); (h) Relationship of F2 over F1.

Domain VI

Domain VI is located north of Masabar village and comprises combinations of F_1, F_2 and F_3 folds. The area depicts meso-scale F_1 folds (Fig. 3.2b), regional scale F_2 antiformal and F_3 synformal structure. Structural data recorded from this domain is S_0, S_1 and S_2, holds parallel relationship with each other. The L_1/ L_2 lineations acquire from the field show an orientation of F_1/ F_2 fold axes as 40^o/ $N75^o$ (Fig. 4.9). The calculated fold axis through contoured π- diagram suggests that the F_1 and F_2

folds plunge 39^{o} in the direction of $N73^{o}$. The overall trend of the axial trace exhibit ENE-WSW direction, which make this particular area more interesting. The said trend of the fold axis/ axial trace is not seen in other parts of this sector. Hence it would not be wrong to state that there exists an effect of another fold event over F_1 and F_2 to modify its structural disposition. The data also helped in analysing the F_3 fold developed on regional scale. The results suggest that the F_3 fold axis show the plunge of 64^{o} in the direction of $N5^{o}$. The F_3 synformal structure is found to be developed on long limbs of F_1 and F_2 folds. The manifestation of F_3 over F_1 and F_2 has resulted into drifting of pre-existing fold axis from ESE to ENE direction.

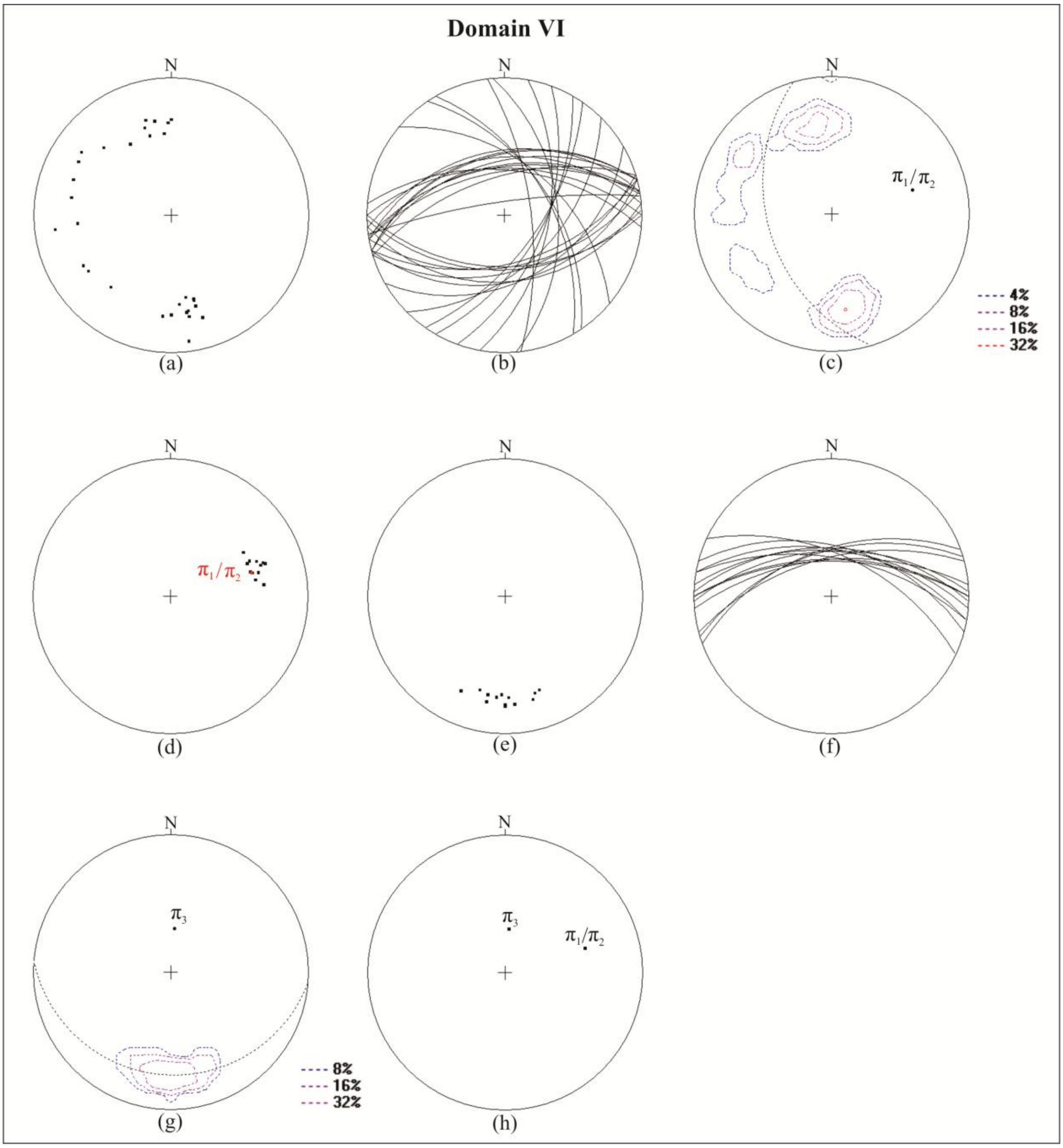

Figure 4.9: **Domain VI**: (a) Poles to planes (S0, S1, S2, n=30); (b) Cyclographic plot (S0, S1, S2, n=30); (c) Contoured pie diagram (4, 8, 16, 32% contours per 1% area); (d) Lineation of F1/F2 (n= 12); (e) Poles to planes (S0, S1, S2, n=13); (f) Cyclographic plot (S0, S1, S2, n=13); (g) Contoured pie diagram (8, 16, 32% contours per 1% area); (h) Relationship of F3 over F1/F2.

4.3 Sector 2: Malabar to Pani

The area within this sector shows derivatives of three fold events F_1, F_2, F_3 (Fig. 4.10). The northern and the western part of part of the present sector is characterised by F_1 and F_2 folds, whereas the F_3 folds are mainly located along the eastern side of the sector. The F_1 folds are second order tight having low wavelength with high amplitudes and F_2 folds are first order open with varying amplitude versus wavelength ratio. The steepness of F_2 limbs increases long the northern and southern part of the sector, respectively. The western part of the sector shows a gentle value of the litho-units in terms of their inclination. The present sector has been divided into seven domains (i.e. from domain VII to XlII).

4.3.1 Structural analyses of Sector 2

Domain VII

Domain VII comprises one antiform and two synforms. The structural data measured in this domain is S_0, S_1 and S_2. There exists subparallel relationship of S_0-S_1, whereas the S_2 foliations are oblique. The S_2 show perpendicular relationship at the F_2 fold hinge, but exhibit an oblique convergence along the limb portions. The domain represents mainly derivatives of F_2 folds in the form of folded thicker litho-units on regional scale. There also exists signatures of F_1 folds, which occur as minor folds within the limbs and hinges of F_2 folds (Figs. 3.3c-d). The plot of S_0, S_1 and S_2 data suggest that the fold axis of F_2 fold plunges 15^o in the direction of N280^o (Fig. 4.11).

Domain VIII

The present domain represents F_1 and F_2 folds. Mesoscopic F_1 folds are less evident as compared to the previous domain. Here F_1 has been refolded on a regional scale to form F_2. The axial trace of F_1 fold can be traced from east of Vishengarh at the north till SE of Kuivav in the south. This axial trace can be marked within quartzites of the Narukot Formation. The structural data recorded from this domain is $S_{0,}$ S_1 and S_2. The western part of this domain is characterized by sub-parallel relationship of S_0-S_1, whereas the S_2 show oblique relationship with respect to the earlier schistosity and bedding. In the eastern part of the present domain, the relationship between S_0, S_1 and S_2 virtually gets sub-parallel to each other. The southern limb of the F_2 fold strikes nearly E-W with southerly dip and the northern limb depicts N0° dip direction with a strike of N90°W. There exists a steep dip of the limbs for F_2 folds along the northern and southern margins of the present sector. The central part of the F_2 fold, where the hinge is located, the dip amount shows gradual decrease in term of its inclination. The lower hemisphere stereographic projection for F_1 fold suggests that the fold axis plunges 47° in the direction of N277°, whereas in case of F_2 fold it plunges 19° with a westerly

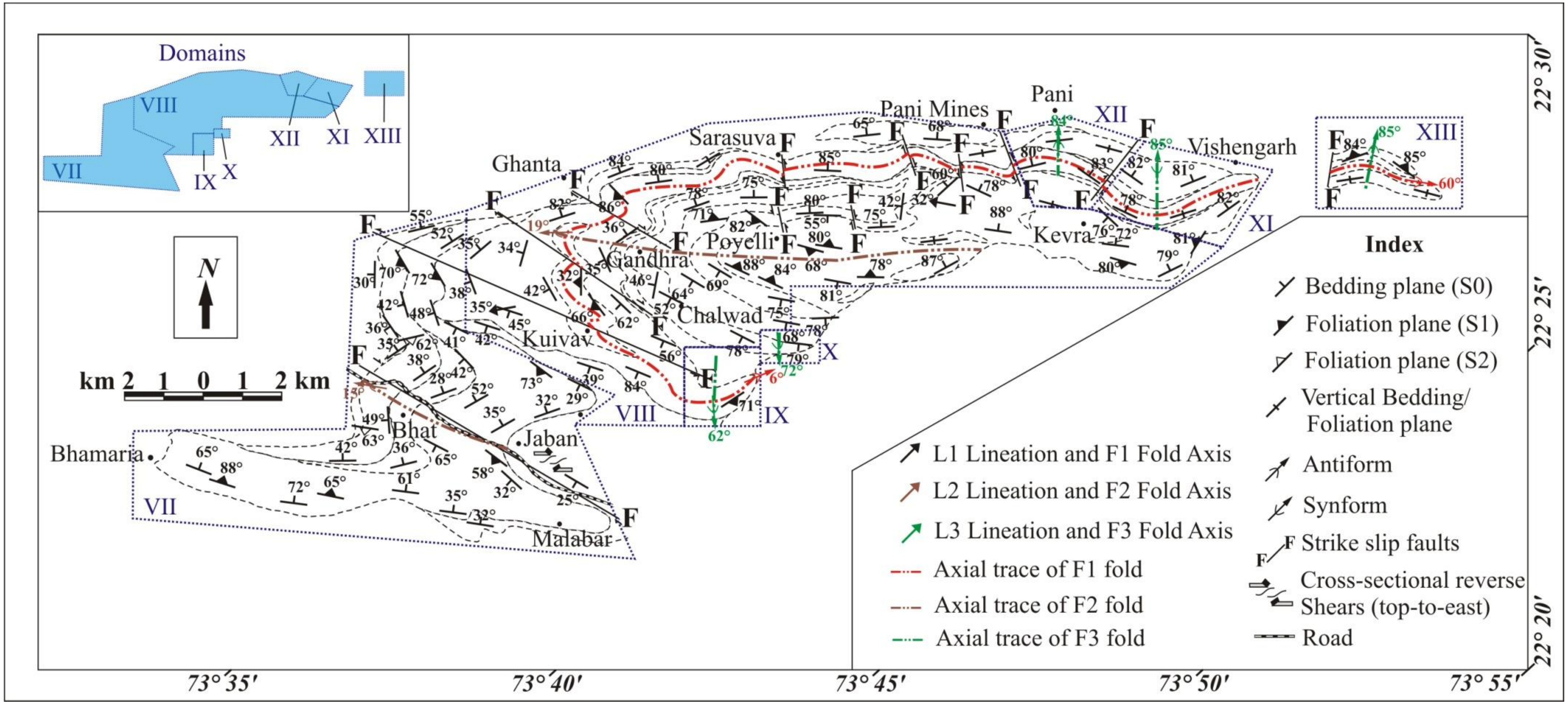

Figure 4.10: Structural Map of Sector 2.

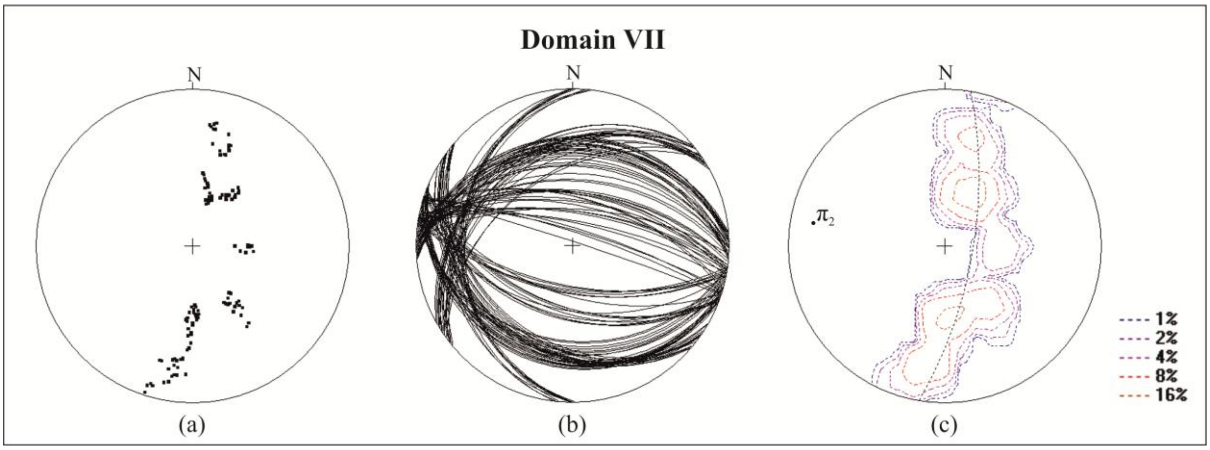

Figure 4.11: **Domain VII**: (a) Poles to planes (S0, S1, S2, n=126); (b) Cyclographic plot (S0, S1, S2, n=126); (c) Contoured pie diagram (1, 2, 4, 8, 16% contours per 1% area).

plunge direction (Fig. 4.12). The relationship of F_2 over F_1 has resulted into steepening of F_1 fold axis. The statistically calculated π_1 and π_2 fold axis falls in same quadrant indicating co-axial deformation.

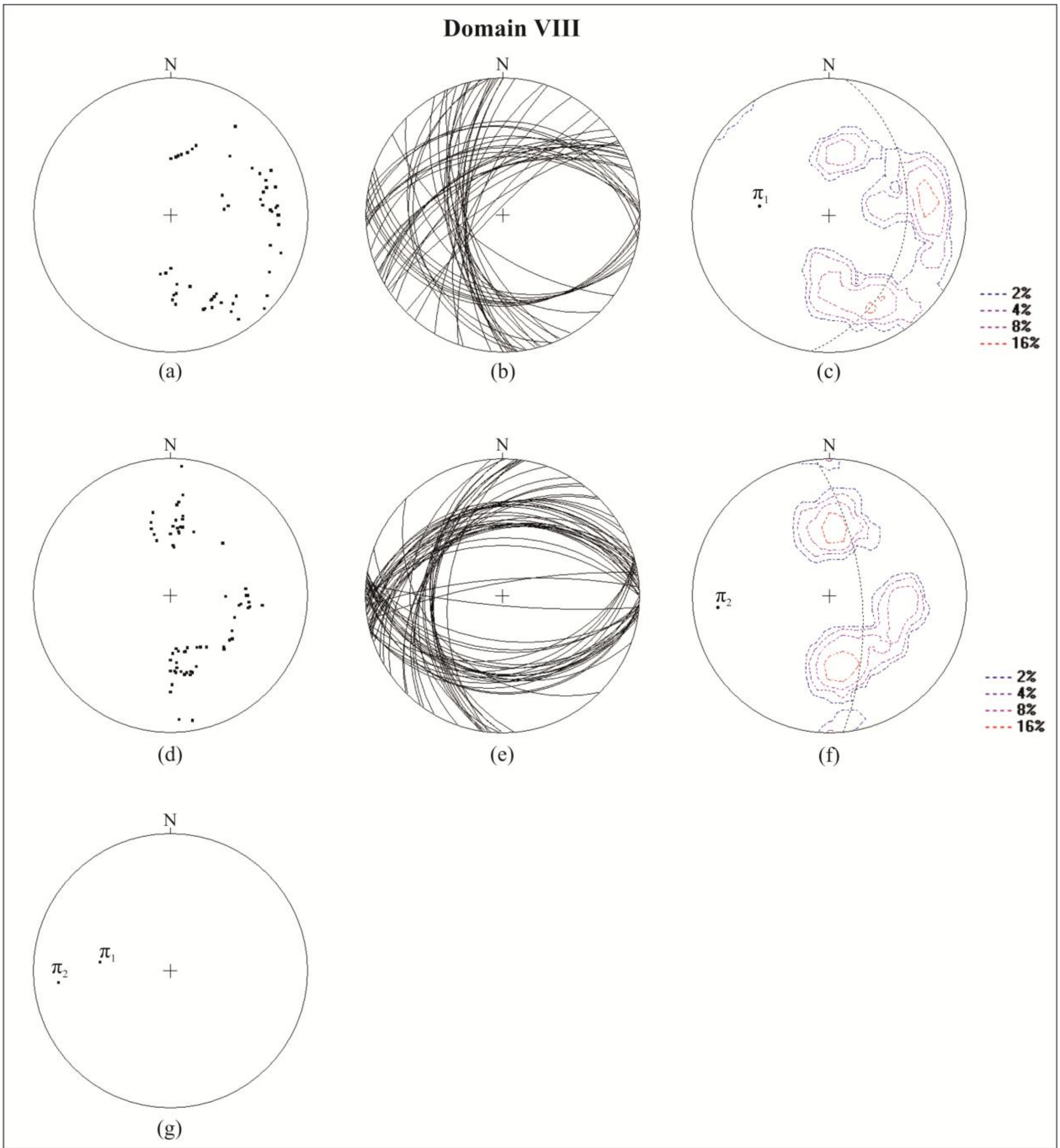

Figure 4.12: **Domain VIII**: (a) Poles to planes (S0, n=54); (b) Cyclographic plot (S0, n=54); (c) Contoured pie diagram (2, 4, 8, 16% contours per 1% area); (d) Poles to planes (S1, S2, n=66); (e) Cyclographic plot (S1, S2, n=66); (f) Contoured pie diagram (2, 4, 8, 16% contours per 1% area); (g) Relationship of F2 over F1.

Domain IX

The present domain represents the relationship between F_1 and F_3 fold. The F_1 fold closure along the eastern part of this domain plunges with an amount of 6° in direction N74°. The refolded F_1 fold has generated regional scale F_3 antiformal structure having plunge due south with an amount of 62°. Here, S_0, S_1 data has been used primarily to study the relationship of F_3 over F_1 (Fig. 4.13) The drift of F_1 fold axis in terms of direction is due to the granitic intrusion located in vicinity of this sector.

Domain X

Domain X located E of Chalwad represent F_3 antiformal structure. Structural elements recorded where bedding plane S_0 and foliation plane S_1. The contoured π diagram plotted with the aid of S_0, S_1 data suggest that the orientation of the F_3 fold axis plunges due N162° with an amount of 72° (Fig. 4.14).

Domain XI

The present domain is located south of Vishengarh and comprises mainly of quartzites. The limb 1 of the F_3 synformal structure strikes ENE-WSW with a dip of 81° due NNW. Limb 2 strikes WNW-ESE having similar dip of 83° in the direction of NNE. The contoured π diagram suggests that the orientation of the F_3 fold axis has an attitude of 85°/ N352°. The axial trace of refolded F_1 can also be traced in the present domain having 32° plunge amount of its fold axis in the direction of N266°(Fig. 4.15).

Domain XII

Domain XII represent F_3 antiformal structure located south of Pani. The limbs of this antiformal structure show almost vertical inclination with a varying strike direction from ESE-WNW to ENE-WSW. The overall geometry of the present antiformal structure represents a neutral fold with penetrating fold axis plunging 84° in the direction of N358° (Fig. 4.16).

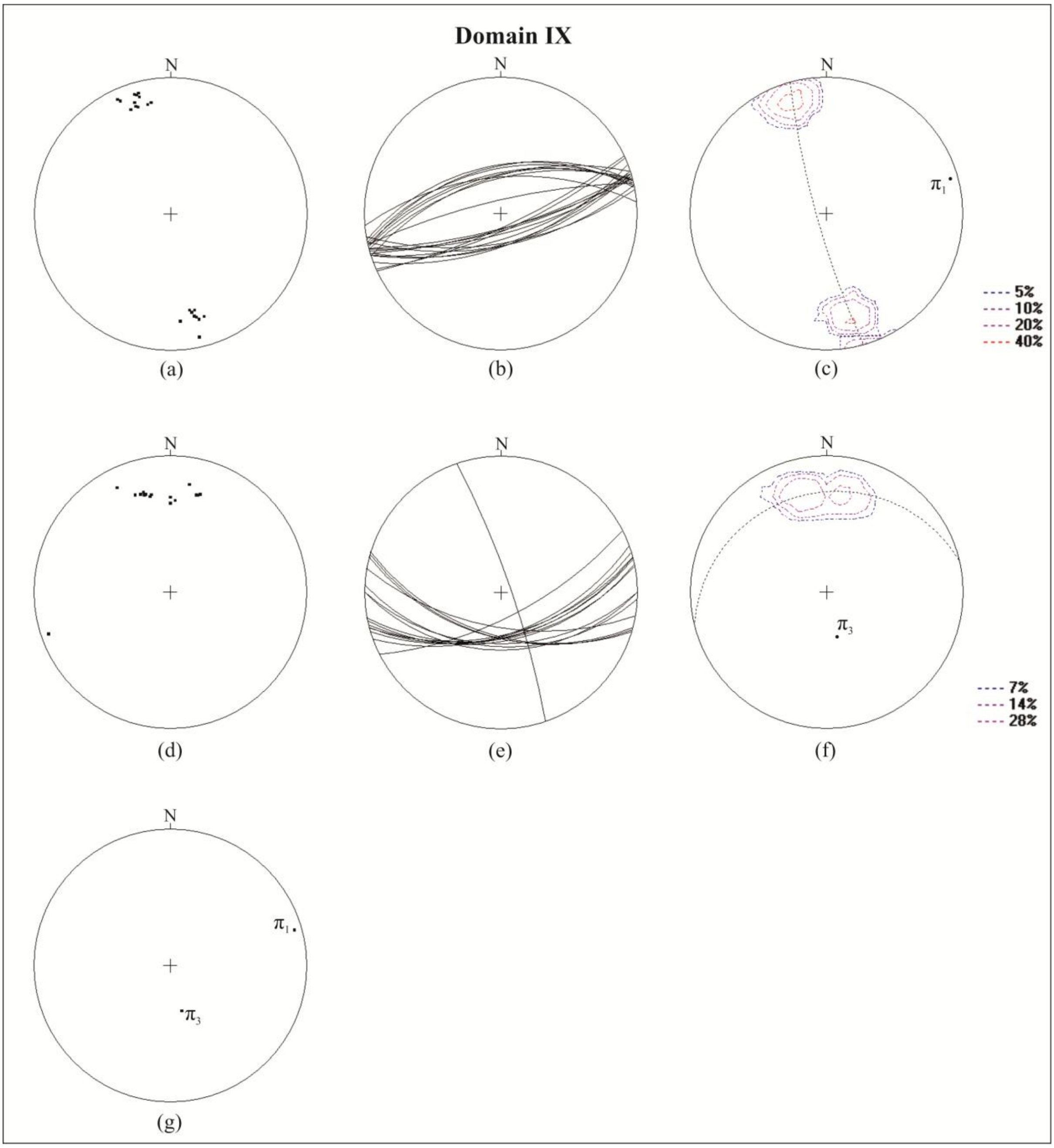

Figure 4.13: **Domain IX**: (a) Poles to planes (S0, n=21); (b) Cyclographic plot (S0, n=21); (c) Contoured pie diagram (5, 10, 20, 40% contours per 1% area); (d) Poles to planes (S0, S1, n=16); (e) Cyclographic plot (S1, S2, n=16); (f) Contoured pie diagram (7, 14, 28% contours per 1% area); (g) Relationship of F3 over F1.

Domain XIII

Domain XIII represents combination of F_1 and F_3 fold on regional scale. The F_1 fold closure can be traced along the easternmost extremity of this sector. The fold closure of F_1 is also characterized by the development of mullions on outcrop scale near Chethapur. The fold axis of F_1 fold plunges 60°/ due N 99°. F_3 folds developed on the km long limbs of F_1 fold forms a regional scale antiformal structure which plunges 85° in the direction of N32° (Fig. 4.17). The statistically derived F_1 and F_3 fold axis through contoured π diagram suggests orthogonal relationship with each other.

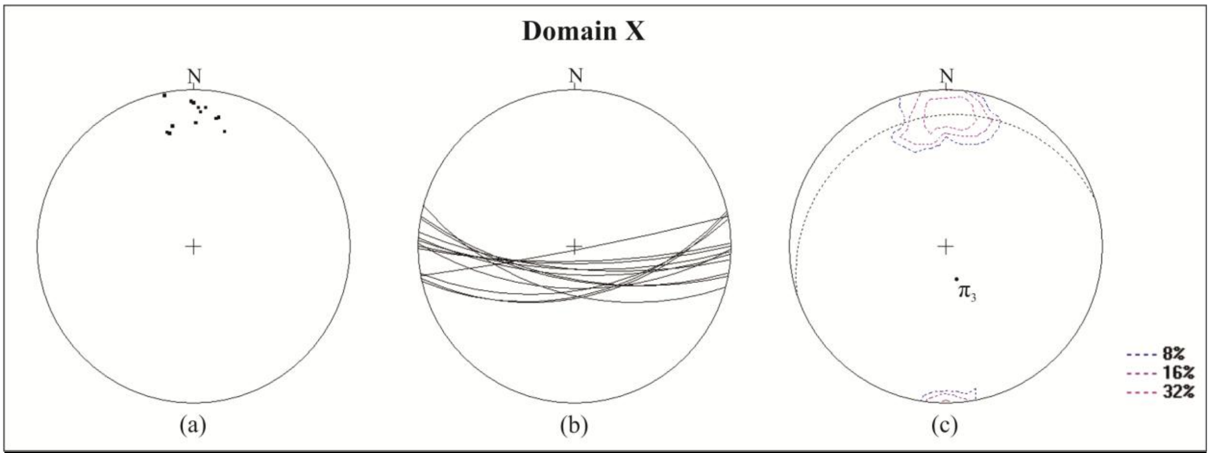

Figure 4.14: **Domain X**: (a) Poles to planes (S0, S1, n=13); (b) Cyclographic plot (S0, S1, n=13); (c) Contoured pie diagram (8, 16, 32% contours per 1% area).

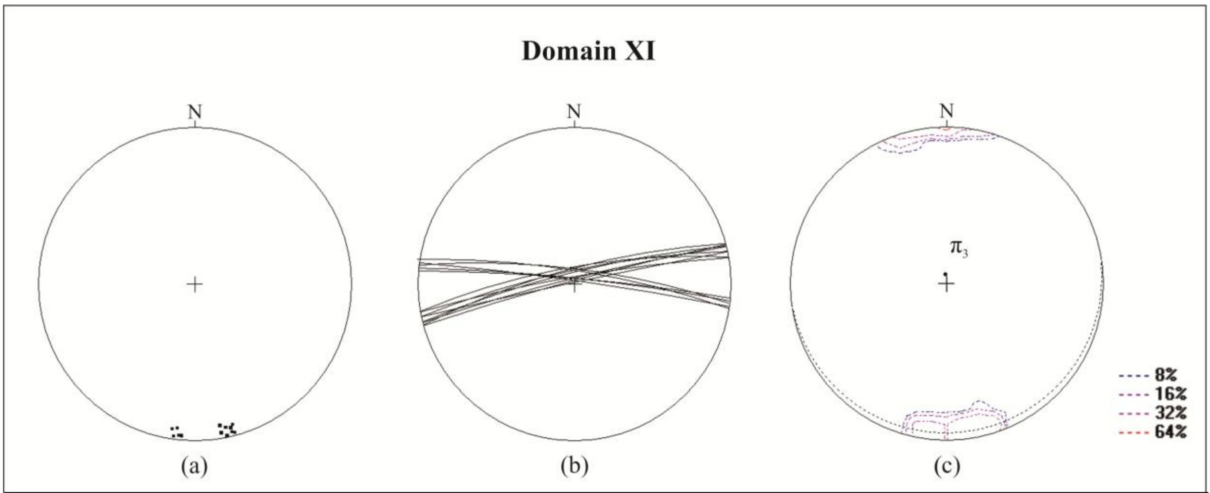

Figure 4.15: **Domain XI**: (a) Poles to planes (S0, S1, n=13); (b) Cyclographic plot (S0, S1, n=13); (c) Contoured pie diagram (8, 16, 32, 64% contours per 1% area).

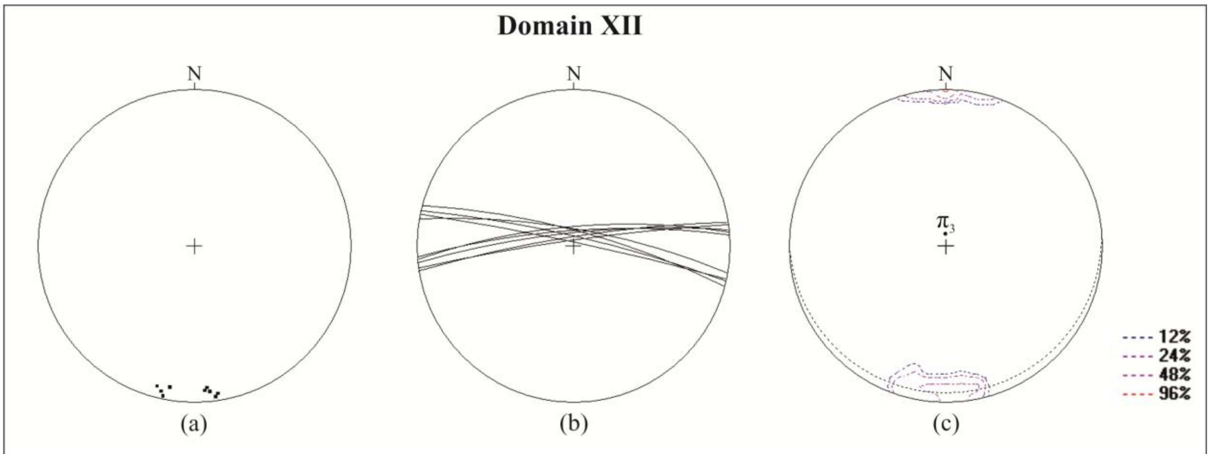

Figure 4.16: **Domain XII**: (a) Poles to planes (S0, S1, n=09); (b) Cyclographic plot (S0, S1, n=09); (c) Contoured pie diagram (12, 24, 48, 96% contours per 1% area).

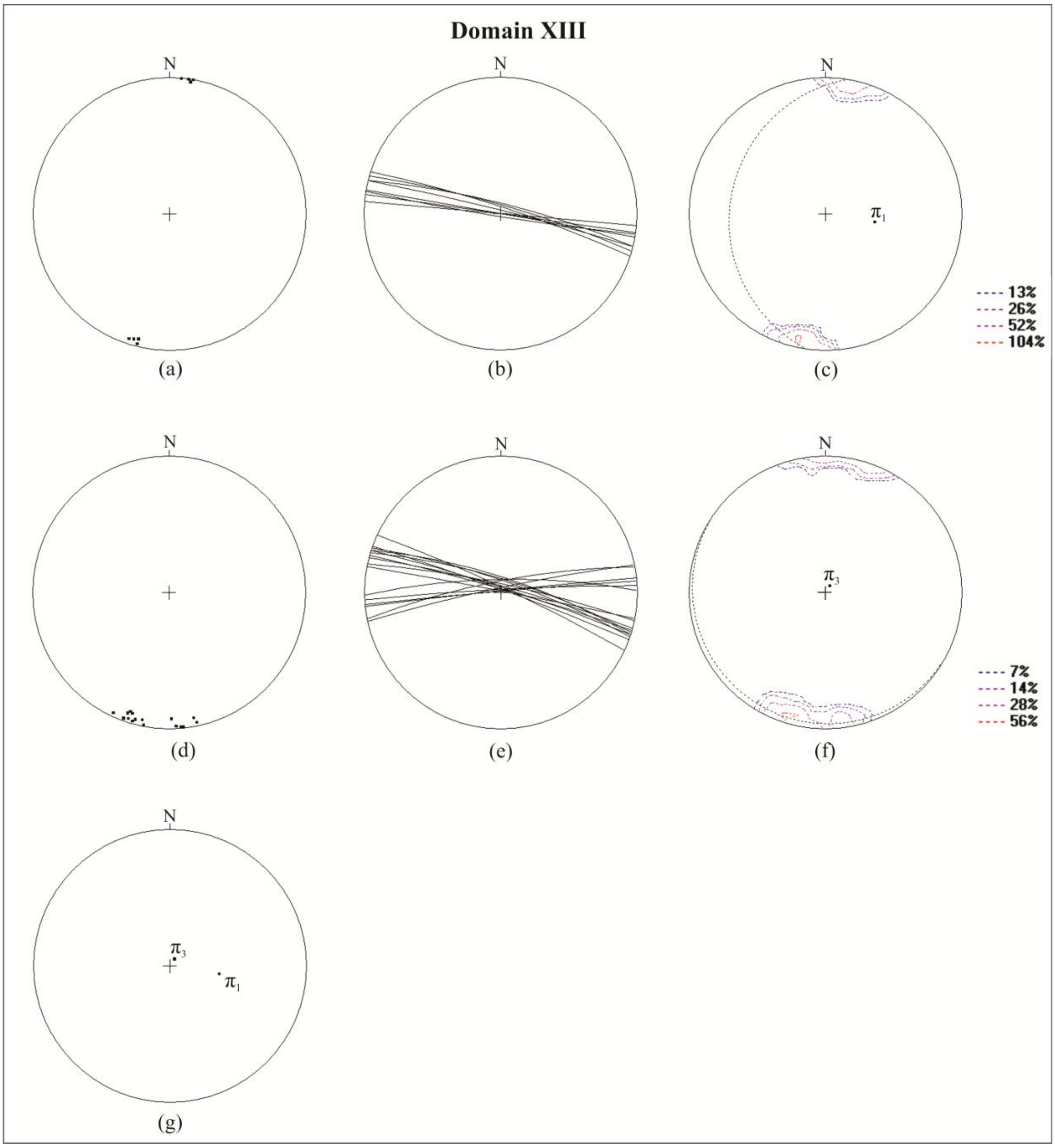

Figure 4.17: **Domain XIII**: (a) Poles to planes (S0, n=08); (b) Cyclographic plot (S0, n=08); (c) Contoured pie diagram (13, 26, 52, 104% contours per 1% area); (d) Poles to planes (S0, S1, n=16); (e) Cyclographic plot (S1, S2, n=16); (f) Contoured pie diagram (7, 14, 28, 56% contours per 1% area); (g) Relationship of F3 over F1.

4.4 Sector 3: Narukot to Wadek

Domal appearance at Narukot has resulted due to interference of F_1, F_2, F_3 folds regionally (Fig. 4.18). In order to carry out the structural analysis the area has been divided into three domains, i.e. XIV, XV and XVI, representing F_1, F_2 and F_3 dominated regions respectively.

4.4.1 Structural analyses of Sector 3

Domain XIV

Domain XIV represent F_1 fold with an axial trace dipping due WNW located at the eastern part of the dome. F_1 fold has resulted due folding of S_0 bedding plane by generating S_1 schistosity plane. Due to the manifestation of F_2 over F_1, S_0 show sub-parallel relationship with S_1 and axial planar S_2 schistosity plane has been developed generating L_2 lineations on S_0 (Fig. 3.6f). These lineations are intersection lineations formed by S_2-S_0 intersection, which plunges 46^o in the direction of N279^o and form pucker axis over the hinge line. By plotting several such lineations over lower hemisphere stereographic projection, the orientation of π_1 axis fits well with the pucker axes lineations obtained from the field. The fold is moderately inclined having pitch of the F_1 fold axis 47^o in the direction of N 280^o (WNW) measured on S_0 plane (Fig. 4.19).

Domain XV

Domain XV comprises tight to isoclinal F_2 folds as F_1 folds refolded along similar trend. The S_0-S_1 relationship is sub-parallel to each other and S_0 dips slightly steeper as compared to S_1. S_2 orientation is feeble and mostly appears as discrete cleavages to form L_2 intersection lineations between secondary cleavage planes and S_0 over S_1. π_2 axis of F_2 fold matches with the data set of intersection lineations recorded from F_2 dominated area. The core of the F_2 fold is traceable for 1 km at the western margin of the Narukot dome in domain XV. The N and the S limb of F_2 strike ~ E-W having due N and due S dip directions, respectively. The fold axis plunges towards W with an amount of 20^o and possess a sub-vertical axial plane (Fig. 4.20).

Domain XVI

Domain XVI has been sub divided in to XVIa and XVIb, which depicts F_3 open fold trending N-S axial trace over km long limbs of F_1 and F_2 fold. The axial plane can be traced from the N to the S fringe of the dome dividing it into two ~ equal portions. Steeply dipping mesoscopic F_3 fold axes has been observed along outer rim near SW of Wadek (Fig. 3.3a). These lineations fit well with the fold axis π_3. The fold possess vertical axial plane and have a northerly plunge of its axis (Fig. 4.21).

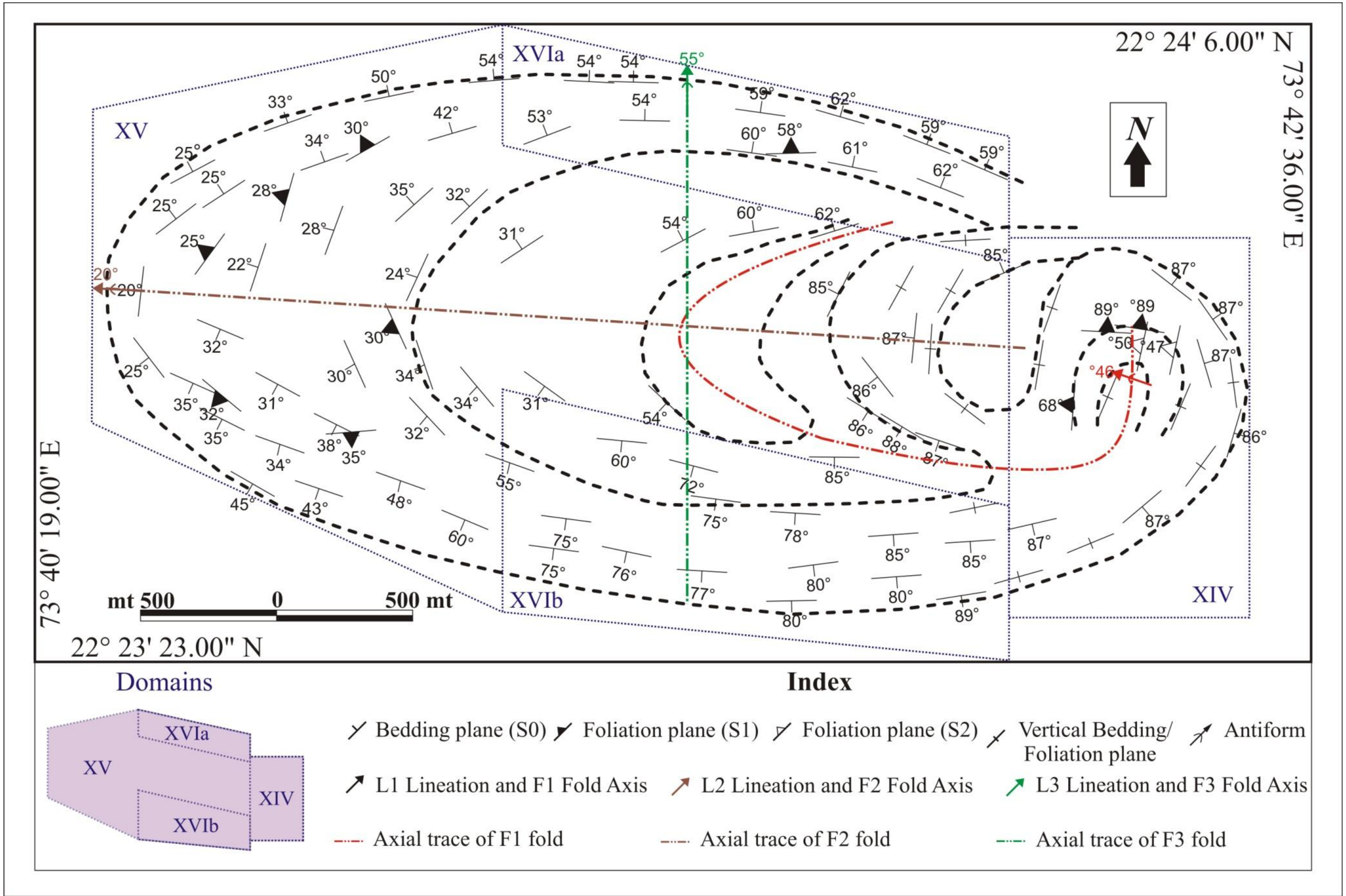

Figure 4.18: Structural Map of Sector 3.

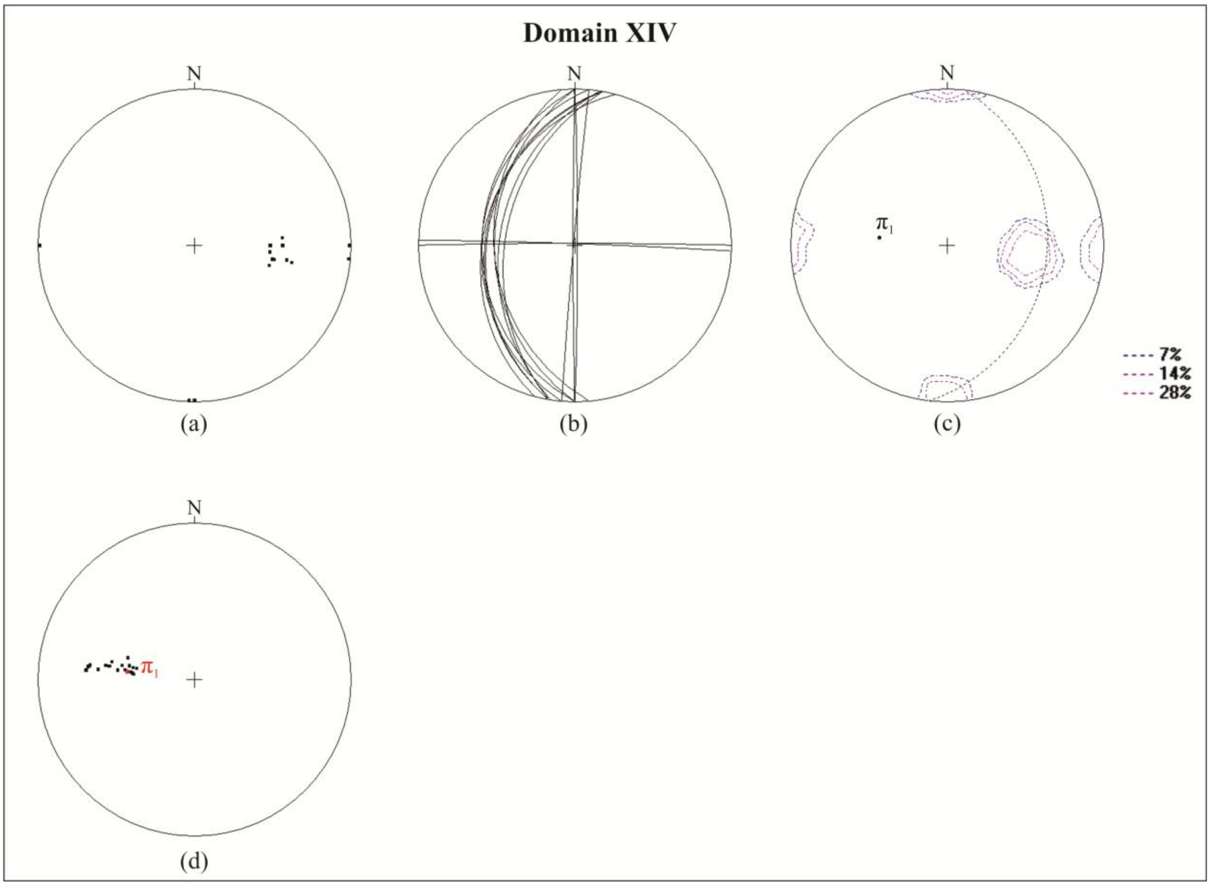

Figure 4.19: **Domain XIV**: (a) Poles to planes (S0, n=15); (b) Cyclographic plot (S0, n=15); (c) Contoured pie diagram (7, 14, 28% contours per 1% area); (d) Lineation data of F1 (n=18).

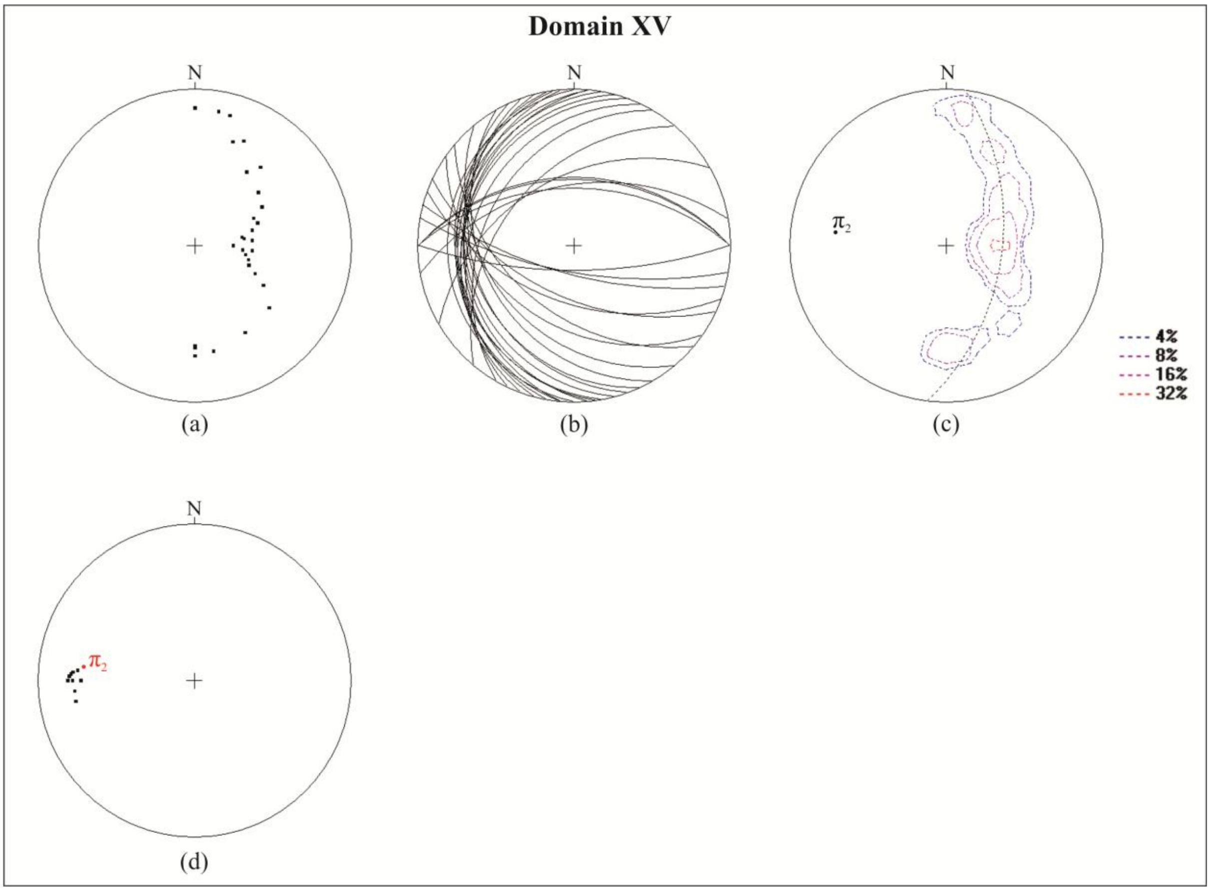

Figure 4.20: **Domain XV**: (a) Poles to planes (S0, S1, n=29); (b) Cyclographic plot (S0, S1, n=29); (c) Contoured pie diagram (4, 8, 16, 32% contours per 1% area); (d) Lineation data of F2 (n=11).

Representation of F_{1-3} folds along with the orientation of the axial plane and fold axis in the Narukot dome, depicted by SRTM worldwide elevation data (3-arc-second resolution) downloaded from Global mapper (v17) (Fig. 4.22).

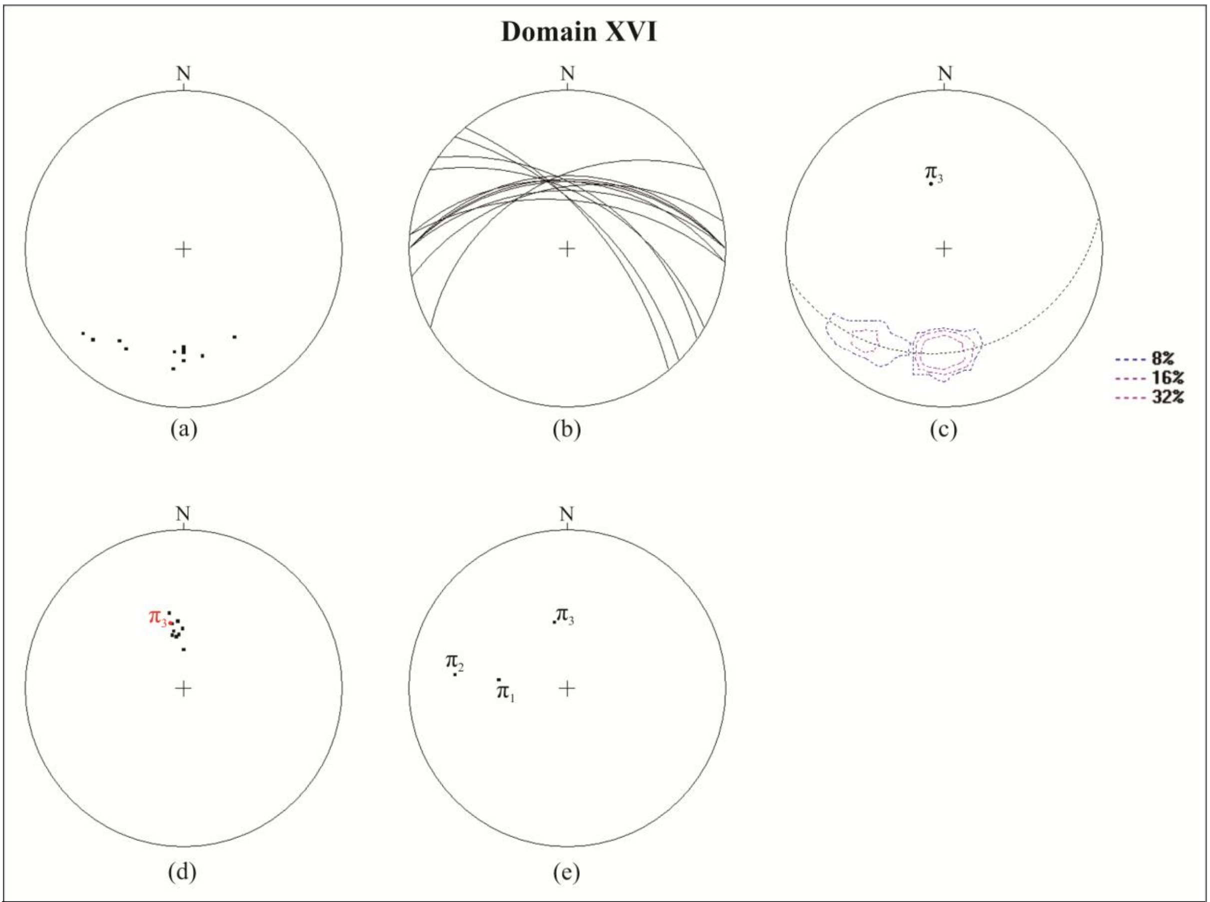

Figure 4.21: **Domain XVI**: (a) Poles to planes (S0, S1, n=14); (b) Cyclographic plot (S0, S1, n=14); (c) Contoured pie diagram (8, 16, 32% contours per 1% area); (d) Lineation data of F3 (n=09); (e) Relationship of F1, F2 and F3 fold.

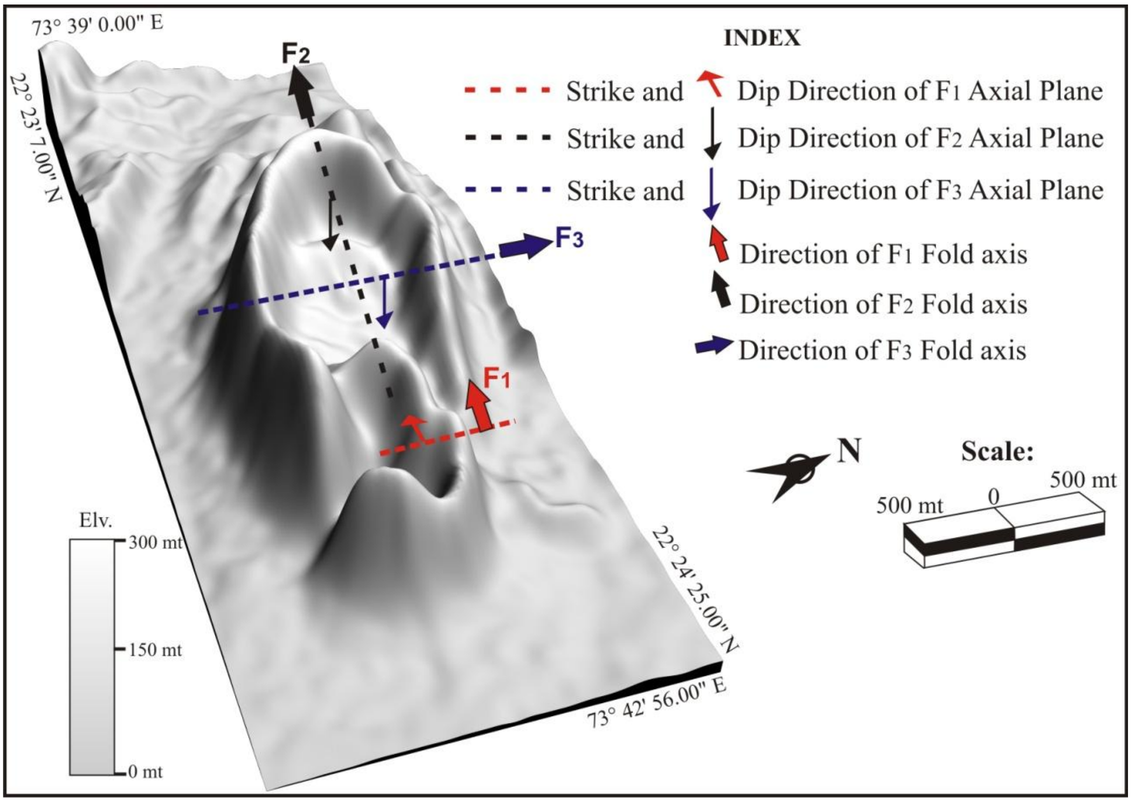

Figure 4.22: SRTM derived shaded relief map of the Narukot Dome. Respective orientations of the axial planes and fold axis has been demarcated.

4.5 Sector 4: Bhamaria to Kanpur

The Sector 4 lies from Bhamaria in the south to Kanpur in the north (Fig. 4.23). The present sector though represents extensive in terms of its extent but there exist scarcity of structural data, as majority of outcrops have been eroded or buried under alluvium. Being phyllite as a softer rock, they have been destroyed for the agricultural practices.

4.5.1 Structural analyses of Sector 4

The present sector represents broad F_2 folds on a regional scale with inter-bedded minor F_1 folds (Fig. 3.5b). At few places the rocks of this sector represent refolded folds (Figs. 3.5c-d) and broad open folds on outcrop scale (Fig. 3.3e). The area is devoid of clear distinction of F_2 fold closures on regional scale; hence it is difficult to divide the present sector into various domains. The author finds it more appropriate to present the data set representing F_1 and F_2 folds unanimously. The structural data recorded from this sector is S_0, S_1 and S_2. S_0 and S_1 show sub-parallel relationship with each other, while S_2 is found to be oblique with respect to S_0llS_1.

The contoured π diagram derived by plotting S_0llS_1 data for F_1 fold suggests that the fold axis plunges 35° in the direction of N281°. The L_1 lineation data collected from this sector also matches with the statistically derived F_1 fold axis. Regional scale F_2 fold axis calculated by plotting S_0, S_1 and S_2 shows plunge of 51° in direction of N272° (Fig. 4.24).

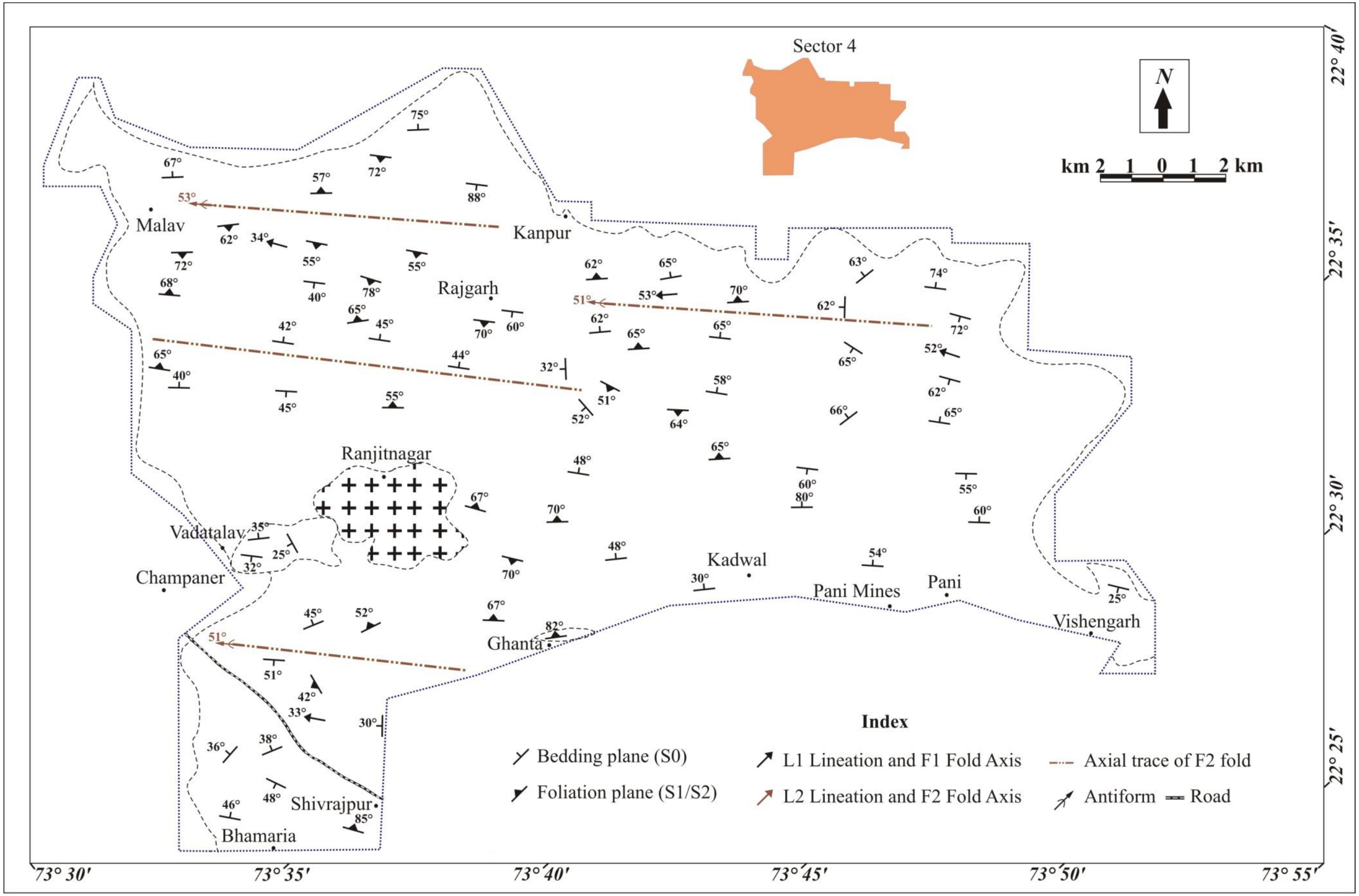

Figure 4.23: Structural Map of Sector 4.

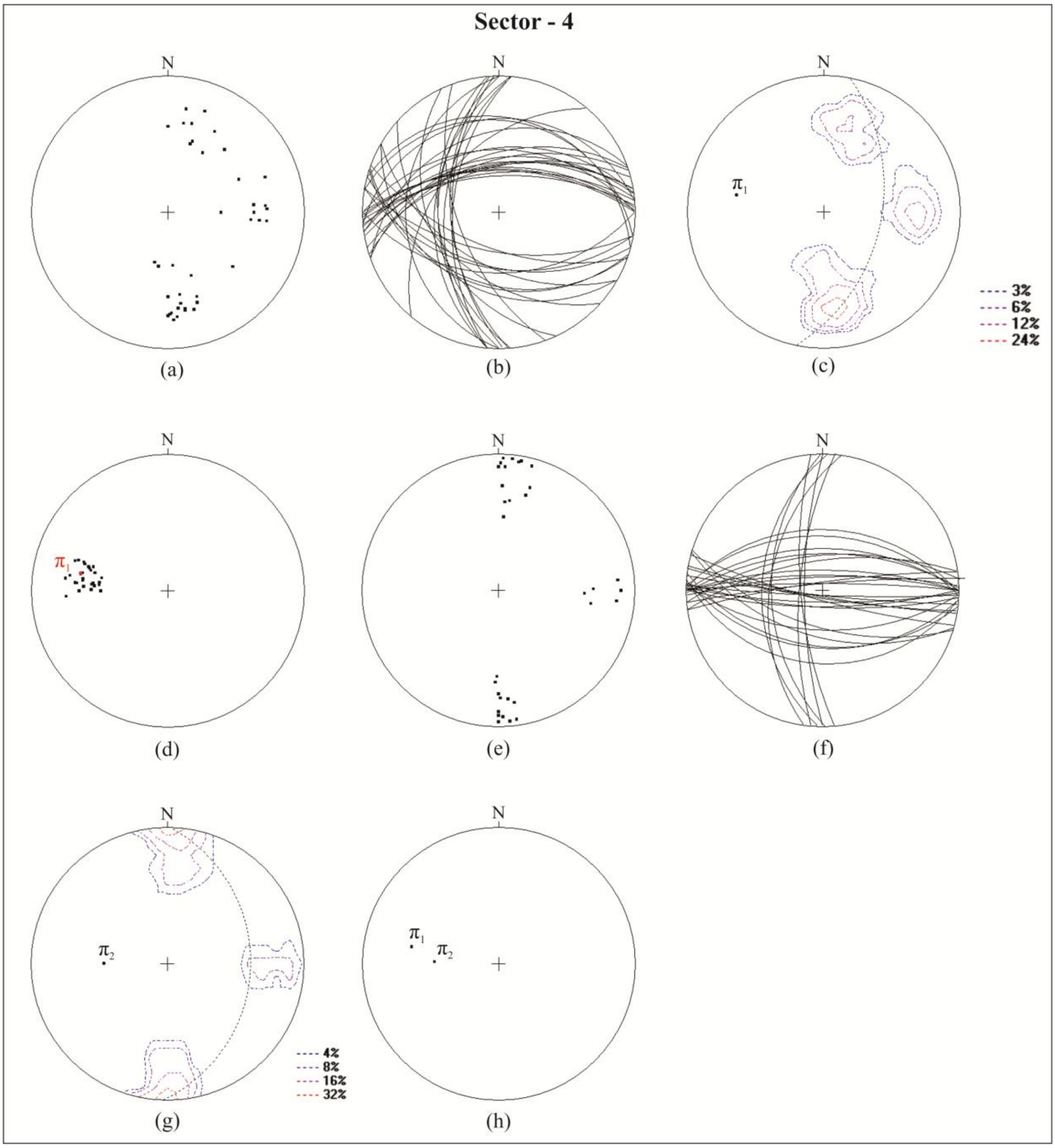

Figure 4.24: **Sector 4**: (a) Poles to planes (S0, S1, n=40); (b) Cyclographic plot (S0, S1, n=40); (c) Contoured pie diagram (3, 6, 12, 24% contours per 1% area); (d) Lineation data of F1 (n=28); (e) Poles to planes (S0, S1, S2, n=32); (f) Cyclographic plot (S0, S1, S2, n=32); (g) Contoured pie diagram (4, 8, 16, 32% contours per 1% area); (h) Relationship of F2 over F1 fold.

4.6 Sector 5: Isolated patch at Goldungri near Jothwad

As shown in the geological and structural map of the Champaner Group, sector 5 is an isolated patch located at the eastern part of the study area at Goldungri near Jothwad. Based on the map presented for the Sector 5 (Fig. 4.25) it is clear that the area shows deformed calc-silicate rock at the centre followed by thin rim of granite having enclaves of calc-silicate rock (Fig. 3.7a), which further grades into massive, medium to coarse grained leucocratic granite. Due to the small geographic extent of sector 5, the mapping has been done on 1: 10,000 scale. The reading acquired from this patch has been demonstrated collectively.

4.6.1 Structural analysis of Sector 5

The rocks are poly-deformed and exhibit two sets of fold, viz., F_1 and F_2. The northwestern and the southern parts of sector 5 depict mesoscopic rootless tight/ isoclinal F_1 folds (Figs. 3.7d-e). The axial plane in the northwestern part strike NW–SE and fold axes plunges in the direction of N120° with an amount of 50°, whereas in the southern part of the sector 5, trend of the axial plane is N–S and fold axes plunges due N with an amount of 52°. By plotting poles of mesoscopic F_1 fold axes collected from the entire sector 5, F_2 axial trace has been projected by using lower hemisphere stereographic projection (Fig. 4.26). F_2 fold is broad open type synformal structure trending NE–SW and fold axes plunges in the direction of N30° with an amount of 62°. Combination of F_1 and F_2 has generated mushroom shaped outcrop pattern (Fig. 3.7f). The trends of F_1 and F_2 in the present sector (i.e. F1~ NW-SE to N-S and F2~ NE-SW) are unmatched with the present structural trends observed within all other sectors of the Champaner Group. Hence, it would not be wrong to state that the fold event resulted in shaping the F_1 and F_2 trends are possibly out-of-sequence. As these folds are rootless, the granite associated within the limits of this sector has played a dominant role is redefining the surface structural grain of these rocks.

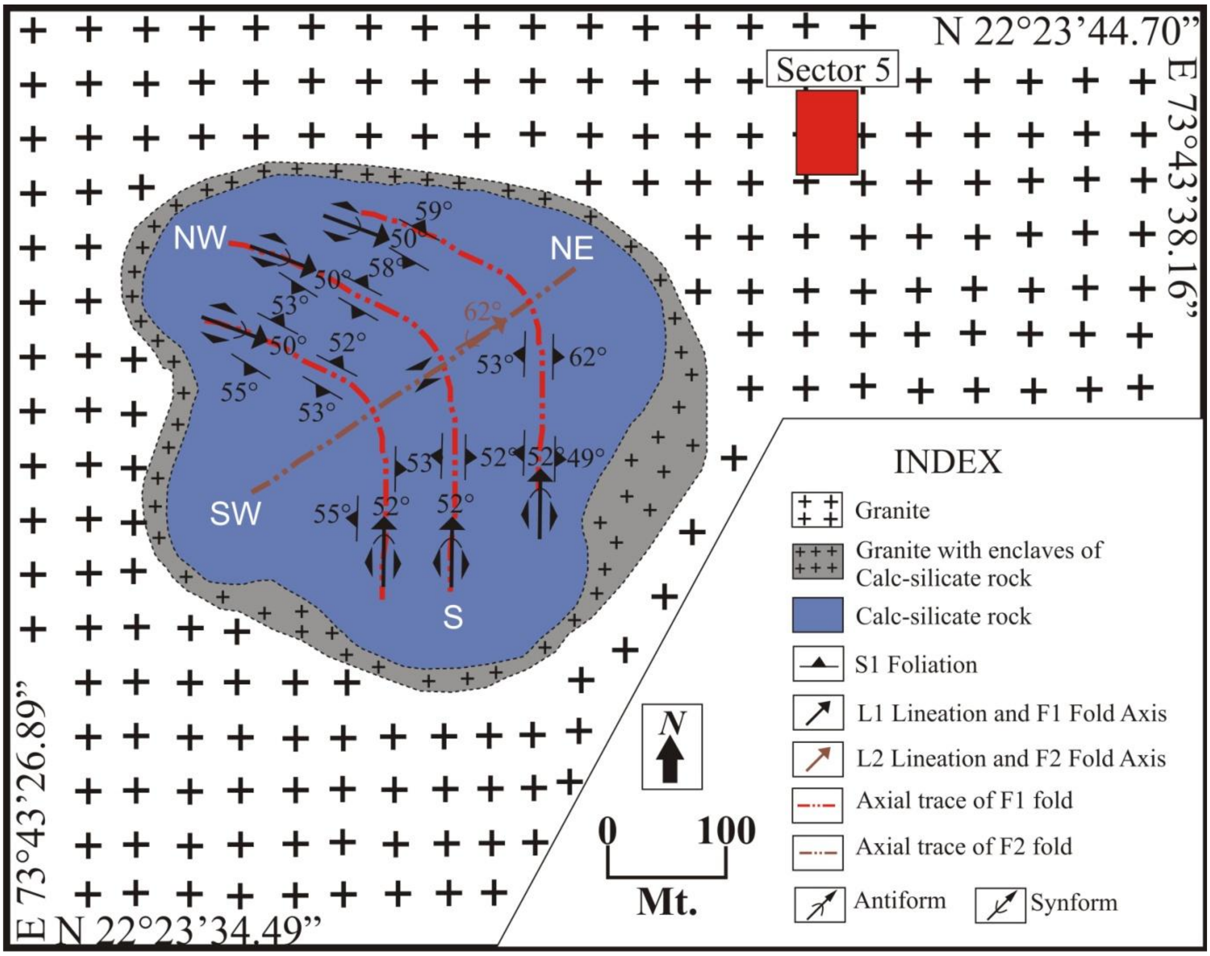

Figure 4.25: Structural Map of Sector 5.

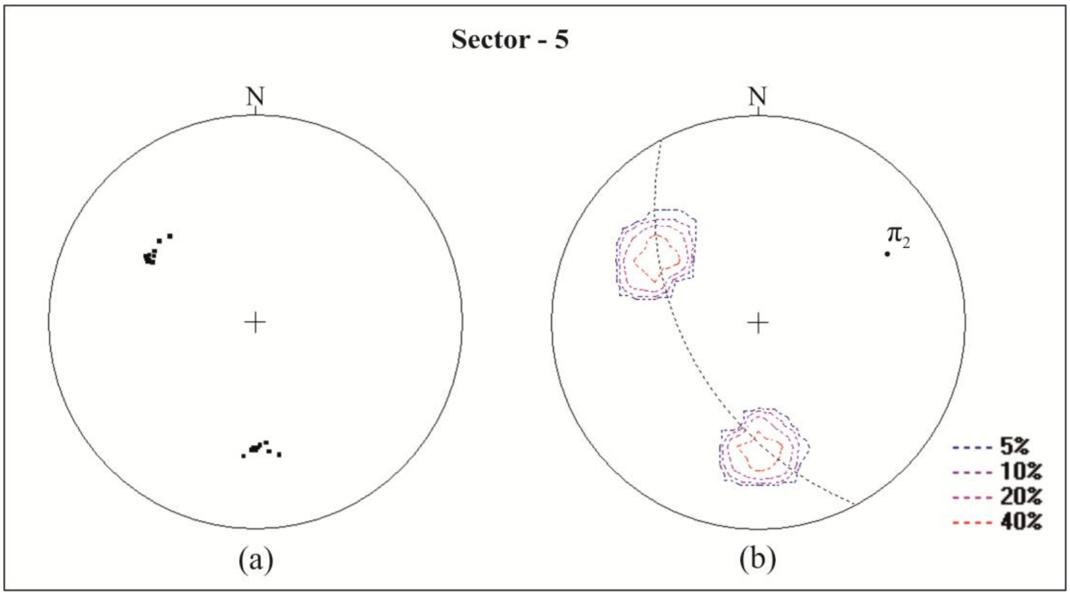

Figure 4.26: **Sector 5**: (a) Poles of F1 fold axes acquired through field, n=22); (b) Contoured pie diagram (5, 10, 20, 40% contours per 1% area).

4.7 Amplitude versus wavelength ratio of folds

F_1, F_2 and F_3 fold episodes within the Champaner terrain, have generated folds with varied amplitude versus wavelength ratio. The results signifies that the folds located west of the Narukot dome near Bhat and at south around Jhand, F_1 fold exhibit second order tight and F_2 folds as first order open with varying amplitude versus wavelength ratio (Figs. 3.2a-b; 3.3c-e; 3.5b). The ratio for F_1 folds has been calculated in the field as the folds are meso-scopic in nature. The ratio ranges from 2:1 to 3:1, obtained along 3-4 mt length across 3-6 sq mt area. However, for F2 folds the ratio ranges from 1:4 to 1:5, obtained along 1-2.5 km length across 0.5-1.5 sq km area. Similarly, for F_3 folds it ranges from 1:3.5 to 0.3:3.0, obtainted along 3-5 km length across 1.5 to 10 sq km area. These F_2 and F_3 fold ratios have been acquired through satellite image and validated during mapping. F_3 fold gradually die out in the form of mega-scale open wraps to meso-scale kink bands (Fig. 3.2c) from eastern to the western stretch of the Champaner Group, respectively.

4.8 Brittle and ductile faults/ shears

Based on the structural map of the study area (Fig. 4.2), it is certain that the Champaner Group has undergone sinistral/ dextral brittle faulting ubiquitously. Outcrop scale evidences of these faults are in the form of fault breccia, fault gauge and tensional gashes (Fig. 3.4b, e and 3.8f). Beginning from the southernmost part of the study area near Rustampura, the fault trends nearly E-W direction, south of Chipat it attains a direction of WNW-ESE, progressing towards the central part of the Champaner Group the fault direction show gradual change of approximate 20^o and finally the fault lying east of Vishengarh show N-S trend. The sway of faults point toward a common origin, lying SE of the study area. Moreover, the directions of these brittle faults depict a coherency in terms of all major axial trace trends of F_1, F_2 and F_3 folds. The present setup hint towards a fact that these faults are developed later than all episodes of folding, experienced by the Champaner Group.

As mentioned in the structural analysis of various sectors, the F_1 and F_2 folds within the Champaner Group plunges due WNW and W direction respectively. The folds having N-S axial traces exhibit their plunge either due N or S. Moreover, doming up of sequences within the limits and along the margins of the group is also evident. Based on the above facts the role of granites to shape the current architecture of faults can be framed. The granitic pulse emplaced after the fold episodes, uplifted the Champaner metasediments from SE and E, which resulted into slippages along pre-defined axial planes and weak zones present throughout the group. The manifestation of strike slip faults in cross-section has resulted in to top-to-east reverse shears (Fig. 4.27). Such evidences are peculiarly seen around the outer periphery of the Narukot dome in quartzites and phyllites (Fig. 3.3b, 3.5f).

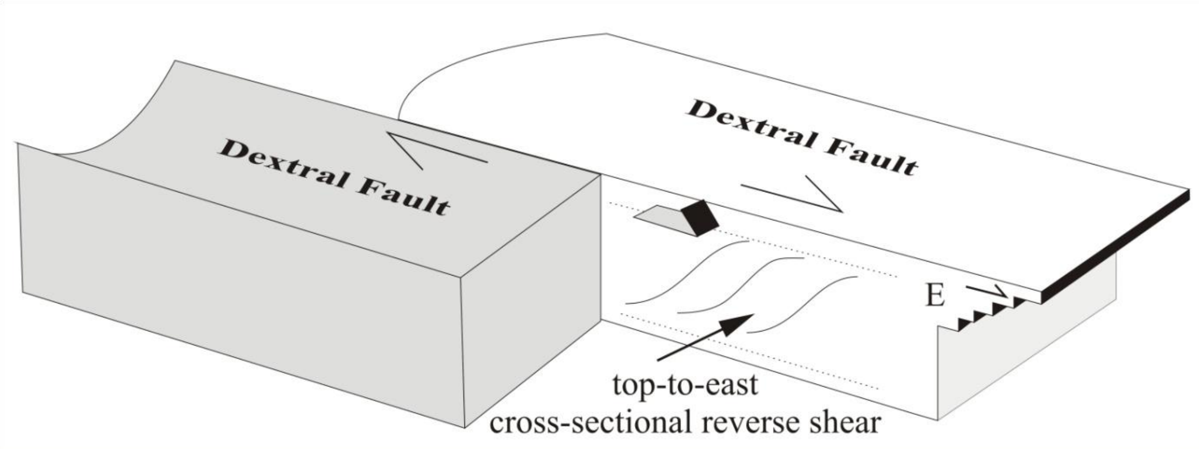

Figure 4.27: Sketch depicting dextral fault in top view, where as top-to-east reverse shear in cross-sectional view. The sketch signifies the transfer of faults from strike slip to reverse in single fault episode, diagram (after, Fossen, 2010).

4.9 Structural Syntheses

On the basis of structural analyses of sixteen different domains within three sectors and in case where, domainal division was difficult, considering them as two separate sectors helped the author to differentiate various fold trends across the Champaner Group. These various fold trends were categorised under respective deformational events. Combinations of more than one fold event have led to the development of interference fold patterns on regional as well as on mesoscopic scale. The present part highlights the overall structural picture emerged from the analysis of data carried out in previous sections.

1. The Meso-Proterozoic rocks of the Champaner Group represent three phases of deformation, viz. D_1, D_2 and D_3.
2. The three phases of deformation have resulted into F_1, F_2 and F_3 folds, respectively.

3. D_1 - D_2 resulted into F_1- F_2 are coaxial having ESE-WNW and E-W trend, respectively, while the D_3 show folds having NNW-SSE to NNE-SSW trend.
4. Combinations of F_{1-3} folds have resulted into various interference fold patterns on regional as well as on the outcrop scale.
5. The area located east of Jaban, near Narukot (Sector 3) shows evidences of superposed folds generated on account of F_1, F_2 and F_3 fold events on a regional scale. Combinations of F_1 and F_2 have generated Type III (hooked shaped) pattern of Ramsay and Huber, (1987), whereas amalgamation of F_3 over F_1, F_2 has developed Type I (dome and basin) interference geometry on a megascopic scale. The Narukot dome is unique because it demonstrates a comprehensive hammerhead anticlinal structure, where the fold axes of F_1, F_2 and F_3 plunges towards due WNW, W and S direction respectively.
6. The derivatives of F_1 and F_2 folds exist in other parts of the study area. The area located within Sector 1 shows derivatives of F_1 fold as mesoscopic tight/ isoclinal and F_2 folds as first order open (Figs. 3.2a-b). The plunge direction of F_2 folds in western part of the sector is due west (domain IV), whereas that of eastern part is due east (domain V), suggesting regional scale Type 1 geometry. The present geometry has resulted on account of uplift due to the granitic intrusion located west of Jhand.
7. The area located within sector 2, exhibit evidences of F_1 folds as second order tight within the limbs of first order open F_2 folds (Fig. 3.3c). The plunge direction of F_1 folds is due WNW and F_2 is due west.
8. The western part of the study area (Sector 4) depicts mesoscale Type III interference pattern within phyllites. F_2 folds are develop by refolding F_1 and are clearly evident on an out crop scale at Kakalpur (Figs. 3.5c-d).
9. The eastern part of the study area (Sector 5) depicts mesoscale F_1 folds (F_1 ~ NW-SE to N-S) and megascale F_2 fold (F_2 ~ NE-SW). These folds are rootless and have no continuity in the sub-surface. Fold interference pattern generated on account of combination of F_1 and F_2 folds are Type-2 over Type-0 (i.e., non-plane non-cylindrical over plane non-cylindrical folds).

These trends and patterns are unmatched with the structural setup of the Champaner Group and are possibly out-of-sequence.

10. F_3 folds within the Champaner Group are mainly restricted at the eastern and the southern periphery in the form of broad open folds developed over kilometre long limbs of F_1 and F_2 folds.
11. The derivatives of F_3 gradually die out in the form of megascale open warps to mesoscale kink bands from eastern to western parts of the Champaner Group, respectively.
12. The amplitude versus wavelength ratio across the Champaner Group, for F_1 ranges from 2:1 to 3:1, obtained along 3-4 mt length across 3-6 sq mt area. In case of F_2 folds the ratio ranges from 1:4 to 1:5, obtained along 1-2.5 km length across 0.5-1.5 sq km area. Finally, for F_3 broad open folds it ranges from 1:3.5 to 0.3:3.0, obtained along 3-5 km length across 1.5 to 10 sq km area, where as for F3 kinks the ratio is 1:4, acquired along 20 cm length across 200 sq cm area.
13. After the fold events, the rocks of the study area have also experienced brittle faulting ranging from E-W to N-S direction in the form of radial pattern. These faults have developed along the pre-defined axial traces due to the granitic emplacement along the SE and E extremity of the study area. Manifestation of strike slip faults in cross-section has resulted in to top-to-east reverse shears. Such evidences are clearly seen around the outer periphery of the Narukot hammerhead anticlinal structure.

4.10 Anisotropy of Magnetic Susceptibility (AMS) studies

When a magnetic field is applied to any material, it produces a magnetization in the parallel or opposite direction of the applied field, which is referred to as “induced magnetization” (M). M is directly proportional to the strength of the applied field (H) and can be given by the formula as:

$$M = KH,$$

Where, M = the magnetic dipole moment per unit volume (A/m), K (proportionality constant) = the magnetic susceptibility and H = the magnetic field strength (A/m).

The equation can be rewritten for magnetic susceptibility as:

$$K= M/H$$

The final value of K is a dimensionless quantity and is represented as SI units.

In case of rocks when an external magnetic field is applied, certain minerals show same strength of induced magnetization in all directions and is considered as "magnetically isotropic". On the contrary, there are few minerals in the rocks, which have a different strength of induced magnetization in preferred directions and are termed as, "magnetically anisotropic". Such minerals have an anisotropic magnetic susceptibility, which is called as the AMS. Due to variation in susceptibility in preferred directions there creates susceptibility ellipsoid (Tarling and Hrouda, 1993), having three principal axes – long, intermediate and short. These axes are the principle susceptibility axes represented in SI units as K1, K2 and K3, where K1 ≥ K2 ≥ K3. The axes of susceptibility ellipsoid matches well with the orientation of principal axes of the strain ellipsoid in tectonically deformed rocks (Hrouda and Janak, 1976; Rathore, 1979, Borradaile and Tarling, 1981; 1984; Hrouda, 1982; Borradaile and Mothersill, 1984; Borradaile, 1987; 1991; Borradaile and Alford, 1987; Borradaile and Henry, 1997).

4.10.1 AMS Data

The present section deals with the Anisotropy of Magnetic Susceptibility (AMS) studies carried out on quartzites of the Champaner Group. The aim of the work was to understand the relationship between the bedding (S_0) and secondary foliation (S_1) within the mono-mineralic and non-foliated rock, such as quartzite. The present studies is of paramount importance in understanding the effects of various fold episodes on the rocks of the Champaner Group.

The oriented sampling of quartzites was done from 12 different locations across the Champaner Group and was analyzed for AMS study. These measurements were done using KLY-4 Kappabridge at Department of Geology and Geo-physics, Indian Institute of Technology, Kharagpur (IIT, KGP). The instrument gave the results for the following parameters: (1) the magnitude and orientations of three principal axes of the susceptibility ellipsoid viz. K1, K2 and K3, where K1 ≥ K2 ≥ K3; (2) mean susceptibility (K_m); (3) degree of anisotropy (P_j); (4) shape parameter (T);

Sample No.	Core No.	K_m (10^{-6} SI units)	F	L	P_j	T	K_{max}	K_{int}	K_{min}	K_{max} – D/I	K_{int} – D/I	K_{min} – D/I
SN1	1	4.86	-1.990	1.369	0	0	1.042	0.956	-0.572	286/48	196/0	105/43
SN1	2	16.50	-14.791	1.154	0	0	1.073	0.968	-0.564	327/36	222/21	108/47
SN1	3	10.20	-6.401	1.056	0	0	1.053	0.967	-0.569	289/45	197/2	104/45
SN1	4	-2.60	1.842	3.910	7.549	-0.381	1.074	0.967	-0.573	214/15	317/41	109/45
SN1	5	24.90	12.783	1.121	20.292	0.914	1.075	0.968	-0.571	274/45	11/7	109/45
SN2	1	-2.11	5.715	3.591	20.766	0.154	1.156	0.882	-0.668	321/74	130/15	221/03
SN2	2	6.02	-5.340	1.185	0	0	1.490	0.878	-0.639	337/79	135/10	226/04
SN2	3	3.07	-2.172	1.381	0	0	1.158	0.883	-0.644	318/70	316/20	226/01
SN2	4	0.747	-0.762	1.305	0	0	1.132	0.789	-0.612	314/72	136/18	46/01
SN2	5	15.70	9.623	1.060	14.138	0.950	1.456	0.822	-0.612	318/79	133/11	223/01
SN2	6	16.60	32.990	1.191	62.909	0.905	1.159	0.829	-0.662	143/79	315/11	045/02
SN3	1	26.10	2.684	1.085	3.286	0.847	1.215	1.041	0.744	342/20	073/05	176/70
SN3	2	17.90	1.375	1.146	1.594	0.402	1.222	1.038	0.735	273/08	06/21	163/68
SN3	3	13.60	1.455	1.063	1.604	0.718	1.199	1.045	0.748	257/41	126/38	13/27
SN3	4	15.30	2.053	1.142	2.501	0.689	1.213	1.048	0.732	266/01	356/20	172/70
SN3	5	34.90	2.503	1.090	3.043	0.828	1.218	1.042	0.736	294/10	027/18	177/70
SN3	6	14.00	1.403	1.024	1.499	0.871	1.212	1.041	0.731	278/12	157/67	12/19
SN4	1	77.50	1.027	1.058	1.089	-0.352	1.037	0.989	0.974	273/11	015/50	174/39
SN4	2	115.00	1.022	1.019	1.042	0.089	1.036	0.929	0.974	268/06	168/59	02/31
SN4	3	132.00	1.019	1.012	1.032	0.250	1.037	0.989	0.974	269/08	165/60	03/28
SN4	4	68.10	1.028	1.063	1.095	-0.374	1.029	0.989	0.973	279/10	22/50	181/38
SN4	5	84.00	1.053	1.057	1.114	-0.035	1.037	0.984	0.974	279/12	20/42	177/46
SN6	1	190.00	1.060	1.021	1.085	0.0479	1.035	1.008	0.957	294/28	56/45	185/32
SN6	2	167.00	1.043	1.026	1.071	0.250	1.032	1.007	0.952	299/35	71/44	189/26
SN6	3	176.00	1.052	1.035	1.089	0.191	1.035	1.008	0.953	307/41	64/28	177/37
SN6	4	188.00	1.059	1.025	1.088	0.390	1.034	1.010	0.957	298/32	58/39	181/35
SN6	5	195.00	1.088	1.017	1.115	0.667	1.033	1.007	0.957	307/37	51/17	161/48
SN6	6	164.00	1.042	1.033	1.076	0.116	1.038	1.006	0.958	299/35	60/36	180/35
CPR1	1	111.00	1.099	1.017	1.127	0.699	1.045	0.999	0.956	084/55	271/35	179/03
CPR1	2	256.00	1.125	1.023	1.163	0.677	1.043	0.998	0.953	087/42	354/03	262/48
CPR1	3	239.00	1.120	1.013	1.149	0.795	1.042	0.996	0.958	090/60	270/31	001/00
CPR1	4	111.00	1.125	1.019	1.160	0.725	1.041	0.997	0.955	039/45	138/09	237/44

Table 4.1: AMS data of the quartzites of the Champaner Group; (K_m = mean susceptibility; F= magnetic foliation; L= magnetic lineation; P_j = degree of anisotropy; T= shape parameter; K_{max}, K_{int}, K_{min} = represent magnitudes of maximum, intermediate and minimum axis of the magnetic ellipsoid, D/I = the direction and inclination of principle axes of magnetic ellipsoid in degrees. '*' mark indicate no results were reflected during the data acquisition.

Sample No.	Core No.	K_m (10^{-6} SI units)	F	L	P_j	T	K_{max}	K_{int}	K_{min}	K_{max} – D/I	K_{int} – D/I	K_{min} – D/I
CPR1	5	148.00	1.150	1.004	1.178	0.943	1.048	0.999	0.957	255/64	087/25	355/05
CPR1	6	105.00	1.116	1.011	1.143	0.814	1.044	0.979	0.956	083/14	256/76	353/02
CPR3	1	29.30	1.335	1.200	1.608	0.226	*	*	*	281/28	13/03	109/62
CPR3	2	29.10	5.702	1.090	7.859	0.906	*	*	*	303/36	209/06	112/53
CPR3	3	5.79	1.152	10102	1.271	0.186	*	*	*	78/16	345/10	226/71
CPR3	4	16.00	1.136	1.062	1.211	0.357	*	*	*	88/60	290/2	195/10
CPR4	1	-2.36	1.306	1.329	1.735	-0.033	-0.030	-0.289	-0.450	333/18	073/30	216/55
CPR4	2	2.34	1.700	1.254	2.174	0.402	-0.032	-0.287	-0.451	264/70	037/14	130/14
CPR4	3	-3.45	1.104	1.533	1.749	-0.625	-0.030	-0.289	-0.450	347/49	096/16	199/37
CPR4	4	-0.872	0.706	-0.728	0	0	-0.030	-0.289	-0.450	084/20	192/41	334/43
CPR4	5	-5.77	1.205	1.189	1.433	0.036	-0.029	-0.285	-0.451	344/58	249/03	157/32
CPR4	6	10.06	1.135	1.165	1.323	-0.092	-0.030	-0.289	-0.450	066/05	331/42	162/47
CPR5	1	27.90	1.303	1.110	1.463	0.434	*	*	*	292/39	77/45	187/18
CPR5	2	13.40	1.268	1.107	1.416	0.400	*	*	*	344/68	84/4	176/21
CPR5	3	16.40	2.581	1.096	3.163	0.824	*	*	*	266/8	14/65	173/24
CPR7	1	4.01	1.202	1.128	1.358	0.210	-0.353	-0.472	-0.975	359/85	102/01	192/05
CPR7	2	5.94	1.171	1.044	1.236	0.571	-0.354	-0.473	-0.975	221/78	312/00	42/13
CPR7	3	4.53	1.158	1.223	1.418	-0.159	-0.353	-0.472	-0.975	153/82	258/02	348/08
CPR7	4	24.00	2.232	1.149	2.764	0.705	-0.353	-0.462	-0.985	255/45	067/45	161/04
CPR7	5	-1.40	1.200	4.541	6.433	-0.785	-0.354	-0.472	-0.975	050/46	243/43	147/06
CPR8	1	89.10	1.013	1.018	1.031	-0.132	1.019	1.066	0.974	059/10	165/57	323/31
CPR8	2	160.00	1.027	1.055	1.085	-0.332	1.020	1.066	0.984	177/00	086/41	267/50
CPR8	3	223.00	1.004	1.108	1.128	-0.924	1.019	1.063	0.974	114/84	317/06	227/02
CPR8	4	224.00	1.086	1.018	1.114	0.640	1.019	1.066	0.974	224/25	052/65	316/03
CPR8	5	159.00	1.131	1.034	1.179	0.575	1.019	1.066	0.969	151/77	358/12	267/06
CPR8	6	121.00	1.013	1.067	1.087	-0.666	1.019	1.063	0.974	151/20	342/70	243/04
CPR8	7	040.20	1.077	1.045	1.127	0.252	1.029	1.066	0.983	130/19	033/20	261/62
CPR9	1	28.40	1.168	1.050	1.237	0.525	*	*	*	310/35	128/55	219/01
CPR9	2	29.00	0.011	1.035	1.049	-0.505	*	*	*	320/37	169/49	61/15

Table. 4.1: Continues.

(5) magnitude of foliation (F) and (6) lineation (L) (Table. 4.1). The mean susceptibility in quartzites has been recorded as 47.37 x 10^{-6} SI units. Some quartzites reveal exceptionally high mean susceptibility values more than 250 x 10^{-6} SI units, due to the presence of mica content. By and large, the quartzites of the Champaner Group reflect low Km values, moreover few samples due to their low Km value do not reflect the values for magnitude of K1, K2 and K3 axis of the magnetic ellipsoid and have been incorporated as asterisk mark * within the table.

4.10.2 Data Interpretation

The orientations of all three principal axes K1, K2 and K3 have been plotted using lower hemisphere stereographic projection (Fig. 4.28). The plane passes through K1 - K2 and essentially matching with K3 pole defines the magnetic foliation (F). The F plane in the given figure is plotted with the dotted line. The stereographic net is also aided with the planar structure S_0 (bedding plane) acquired through field and has been depicted by means of continuous line. There are total 12 samples, viz. SN1-4, SN6, CPR1, CPR3-5 and CPR7-9. Out of which 61 cores have been analysed.

As mentioned in the structural syntheses, the Champaner Group shows three phases of deformation, viz. D_1, D_2 and D_3, of which first two phases were co-axial (F_1 ~ ESE-WNW; F_2 ~ E-W) and the last phase of deformation has N-S trend. The derivatives of all the phases of deformation have been recorded within the quartzites of the Champaner Group. The samples collected from the southern part of the study area, viz. CPR1, 3, 4 and 5 show dominance of F_1 and F_2 fabric. The CPR1 sample has a dominance of F_1 fabric on an outcrop scale due to the presence of mesoscale folds, but shows dominance of magnetic foliation in nearly E-W direction. The superimposition of F_2 fabric over F_1 is clearly seen in the sample collected from NW of Masabar (CPR1). CPR3 sample from the F_2 limb portion show oblique relationship of the magnetic foliation with the bedding. The magnetic foliation trending ENE-WSW direction signifies NNW-SSE shortening direction in the present region. CPR4 and 5 also collected from F_2 limb, depicts similar trend of bedding and magnetic foliation. These samples show the effect of F_2 folds present in the southern part of the study area. The signatures of F_3 fold or preferred orientation along N-S direction are not seen in the present

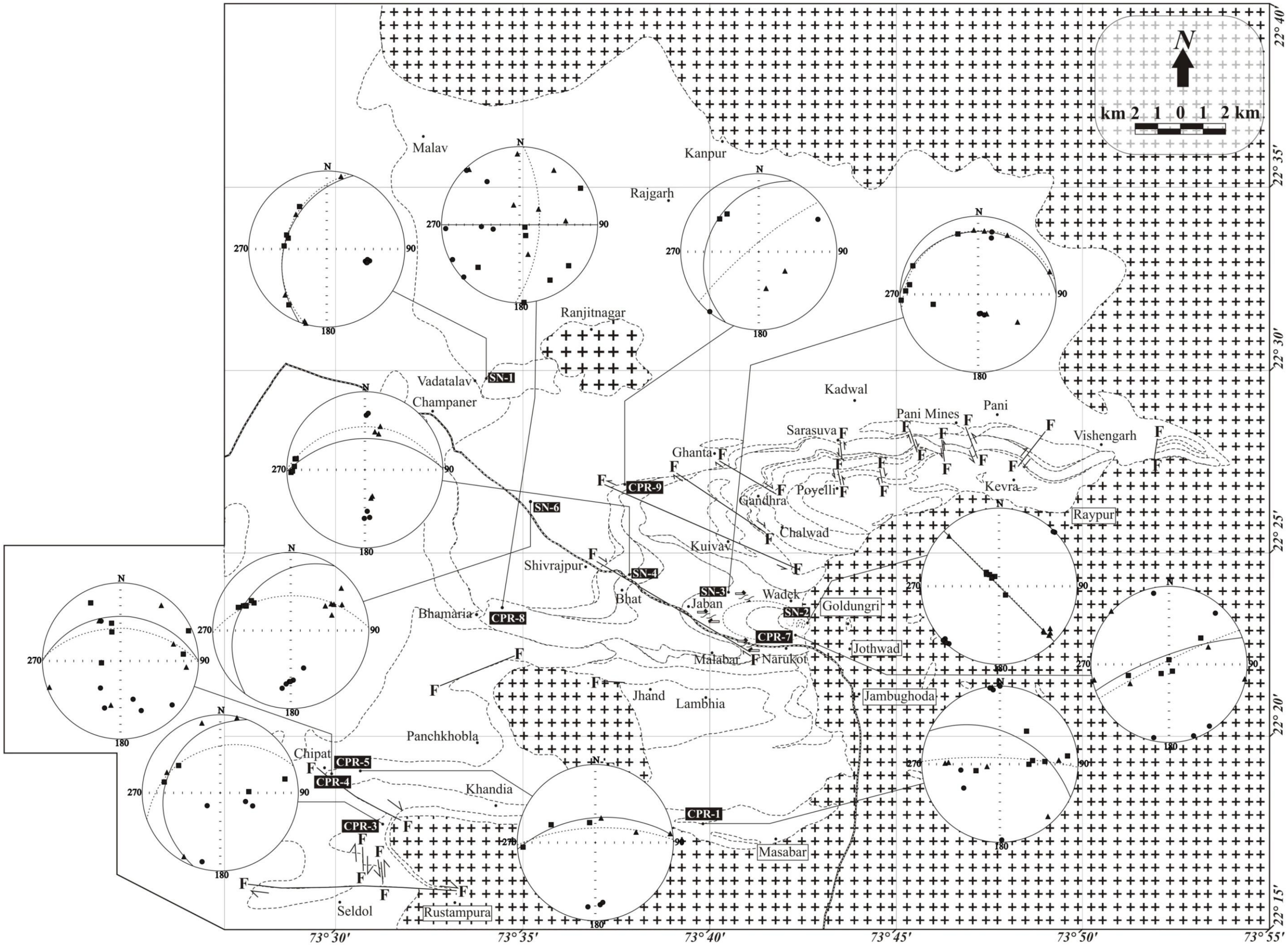

Figure 4.28: AMS orientation data plotted as lower hemisphere projections for the study area. Dotted great circles represent the magnetic foliation, whereas continuous great circles represent the S_0 reading recorded from the field. Filled square, triangle and circle indicate orientations of K1, K2 and K3 respectively.

samples. This suggests that the last episode of deformation did not show any mineral alignment in the southern part of the study area.

CPR 7 and SN2 sample collected from the eastern part of the study area from Narukot dome clearly signifies similar relationship of S_0 and S_1 in these quartzites. The SN2 sample collected from F_1 fold limb and CPR 7 sample from F_2 limb gives nearer results of F_1 and F_2 fabric. It suggests that although, there is a dominance of N-S deformation in the eastern part of the study area, the preferred magnetic fabric parallel to F_3 is absent. Hence the D_3 deformation was not strong enough to modify the magnetic fabric on limbs of F_1 and F_2 folds. Further to the west of the Narukot dome, the samples collected along the axial trace of the F_2 fold (SN3, SN4 and SN6), show prominence of E-W magnetic foliation. The D_2 imprint recorded within these rocks clearly suggests that the central part of the Champaner Group has a dominance of N-S shortening.

The western and northern part of the Champaner Group shows the magnetic fabric parallel to the D_3 deformation of the Champaner Group in the samples viz. CPR 8, CPR 9 and SN1. This magnetic fabric ranges from N-S to NE-SW, however there is no mesoscopic scale imprint of the late deformation in the present localities.

Jelinek plot (Pj vs. T) (Fig. 4.29), suggest that majority of the cores fall in the oblate field (flattening field) and few cores from the quartzites show their affinity towards prolate field (constrictional field). In order to examine the type of strain, the available AMS data has been plotted as Flinn diagram (F vs. L), which holds good correlation with the Jelinek plot.

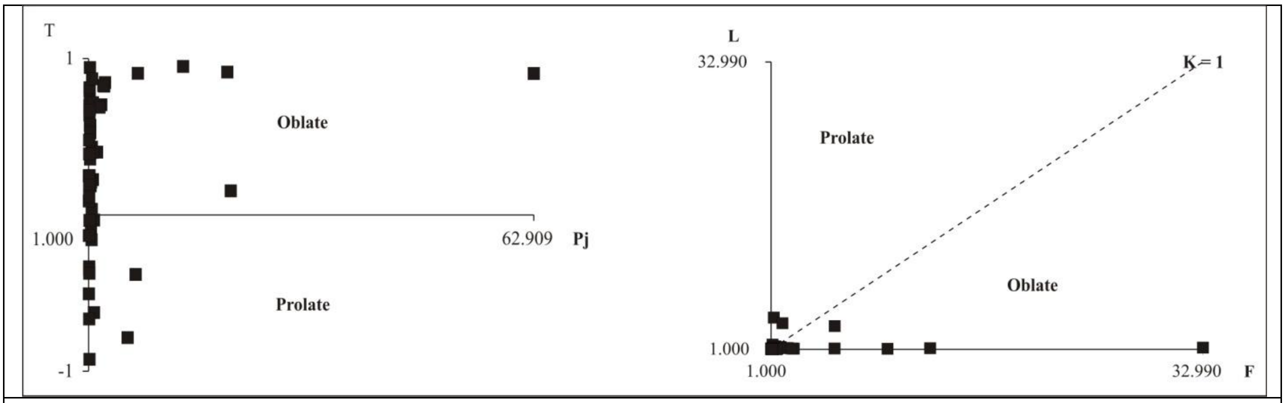

Figure 4.29. Jelinek plots (at left) and Flinn diagram (at right) for the quartzites of the study area.

Most of the AMS data of cores from quartzites of the Champaner Group represented in the Flinn diagram concentrated around K = 1 line, which separates the prolate and the oblate field. This is an indication of the plane strain condition.

----------*END*----------